Inhomogeneous Cosmologies as a Dark Energy Candidate

A Thesis

submitted to
Indian Institute of Science Education and Research Pune
in partial fulfillment of the requirements for the
BS-MS Dual Degree Programme

by

Ramya Narayanan

Indian Institute of Science Education and Research Pune
Dr. Homi Bhabha Road,
Pashan, Pune 411008, INDIA.

December, 2022

Supervisor: Prof. Arijit Bhattacharyay

Certificate

This is to certify that this dissertation entitled *Inhomogeneous Cosmologies as a Dark Energy Candidate* towards the partial fulfilment of the BS-MS dual degree programme at the Indian Institute of Science Education and Research, Pune represents study/work carried out by Ramya Narayanan at Indian Institute of Science Education and Research under the supervision of Prof. Arijit Bhattacharyay, Associate Professor, Department of Physics , during the academic year 2021-2022.

Prof. Arijit Bhattacharyay

Committee:

Prof. Arijit Bhattacharyay

Prof. Prasad Subramanian

This thesis is dedicated to my parents (Latha Narayanan and D. Narayanan) and my younger brother Abhinav.

Declaration

I hereby declare that the matter embodied in the report entitled *Inhomogeneous Cosmologies as a Dark Energy Candidate* are the results of the work carried out by me at the Department of Physics, Indian Institute of Science Education and Research, Pune, under the supervision of Prof. Arijit Bhattacharyay and the same has not been submitted elsewhere for any other degree.

Ramya Narayanan

Acknowledgments

It is difficult to summarize in 250 words the impact various people have had on my five and a half year journey at IISER, Pune. Like the page limit on this thesis, I shall treat the word limit on the acknowledgements as a constitutional requirement that is neither to be acknowledged, nor adhered to.

I must begin, first and foremost, by thanking Prof. Arijit Bhattacharyay for his mentorship and guidance during my nearly two year long project under his supervision. He famously has an *open-door policy*, and I was certainly one to put it to test. From our countless meetings to my incessant and unending questions, his patience and contagious enthusiasm in discussing physics has not only served as an echo chamber to mine, but also made me more confident as an aspiring physicist. I would not be exaggerating when I say that the past two years have been my most enjoyable years of learning at IISER, and he is the sole reason for it. His passion and sincerity to physics as a whole are ideals that I strive to emulate in my career, academia or otherwise.

I would also like to extend my gratitude to Prof. Prasad Subramanian, Prof. Susmita Adhikari and Prof. Arka Banerjee for their helpful inputs and insights as I was navigating my way through fluid dynamics and cosmology for my Master's thesis. My discussions with them served as a significantly more insightful substitute for parsing through pages of lecture notes, textbooks and labyrinthine Wikipedia and stackexchange articles.

I would be remiss to not mention my friends from the fifth year office, or *the physics room*, as we liked to call it. My final year and a half with Rohan, Santhosh, Gautham, Amartya and Praniti were the most enjoyable days of my college life. Our impromptu all-nighters, nights at the CCD terrace (*chhat*), a certain 'expedition' to the Panchvati Hills and our numerous trips to cafes will always be reminisced with pleasant nostalgia. My final months were spent (illegally) at the graduate office with Mohd. Ali, Mayank, Aakash, Ritam, Abhishek and

Aanjaneya, with whom I had enriching discussions on diverse fields of physics. I owe to them my understanding of the nuances of general relativity, non-equilibrium statistical mechanics and any semblance of efficiency in my codes.

I must, finally, thank Prof. Bhas Bapat, who in his capacity as the Dean of Graduate Studies at IISER, Pune during my BS-MS stint gave me unprecedented freedom in the choice of coursework and my completion of the program. I will always be indebted to him for his willingness to allow me to take a risk (that I would like to believe has paid off) at the cost of half a year and potentially his peace of mind.

Abstract

The following thesis attempts to study the effects of inhomogeneity in matter distribution on the average expansion of the universe. The toy models in literature are modified in the direction of generality by inducing a notion of proximity and interaction through shared mass.

Contents

Introduction

The FRW model in cosmology that attempts to model a dynamical universe is based on three fundamental assumptions: 1. The cosmological principle (a statement of homogeneity and isotropy), 2. Ordinary matter (with non-negative pressure) and 3. Ordinary gravity (the Einstein-Hilbert action). While the model successfully describes an expanding universe, it fails to account for an accelerated expansion; contrariwise, it predicts a deceleration. This failure is remedied by the insertion of a cosmological constant, which is tantamount to relaxing the second and third assumptions. This corresponds to adding a term to the matter/source side (as dark energy), or the geometric side of the Einstein field equations (as a cosmological constant), respectively. The effects on spacetime in either case are identical and cannot be distinguished by observation. The FRW universe with a cosmological constant (FLRW) is currently the Standard Model of cosmology.

The effect of this addition serves only to change the way the scale factor in the FRW metric evolves, and given the lack of *direct* observation and theoretical estimate of value, it is pertinent to assume that any other model that similarly modifies the scale factor evolution must be equally valid. The objective of this thesis is to explore alternatives to the FLRW paradigm.

In particular, the thesis aims to study the effects of *inhomogeneous cosmologies*. As the name suggests, this involves relaxing the first assumption made above while leaving the other two unmodified. There is sufficient evidence for the universe being inhomogeneous in galaxy clusters and voids. The FLRW paradigm averages away the inhomogeneities over a homogeneity scale and evolves the averaged quantities via the Einstein field equations. The evolution of inhomogeneities was first dealt with via linear perturbations to the FRW model. This approach falls short in two regards: first that perturbations soon enter a non-linear regime (the linear density contrast of inhomogeneities reaches order unity), and second that linear perturbations do not couple with the net scale factor by construction and hence do

not affect the average expansion. The approach adopted in the thesis are expounded in references [BR12] and [Mag12]; they assume the existence of a homogeneity scale and define a meaningful method for averaging over spacelike hypersurfaces in a covariant manner. The upshot of their argument is that the process of averaging in space and evolving through time do not commute, owing to the non-linearity of the Einstein field equations. The more correct way of dealing with structures would be to time evolve the inhomogeneities and then average over space at every constant-time hypersurface. The effect of the non-commutativity on the expansion in observable, and is termed *backreation*.

References [Räs06a] and [Räs08b] propose toy models which, while somewhat idealistic, prove that inhomogeneities can indeed cause a net accelerated expansion. This approach is more grounded in observable reality, and is hence more promising. This thesis attempts to develop the existing toy models in the direction of generality.

The thesis is structured as follows: Chapter 1 summarizes relevant aspects of the theory of general relativity and introduces the 3+1 Covariant formalism with respect to a set of fundamental observers. A brief mention is made of the various cosmological models and their key results. The main purpose of Chapter 1 is to act as a reservoir of important theorems to be cited later. Chapter 2 covers the FLRW paradigm, discussing its scope and shortcomings. The Friedmann equations are presented with the 3+1 covariant split for easy comparison later. Chapter 3 introduces the Buchert averaging formalism, the Buchert equations that serve to replace the Friedmann equations, and the toy models that make use of these equations to check for an accelerated expansion. Chapter 4 presents improvements to the toy models, and Chapter 5 discusses the results and future work. The thesis is supplemented with appendices to clarify auxiliary concepts and present more involved derivations for completeness.

Chapter 1

Summary of General Relativity

1.1 Introduction and Motivation

Our objective in cosmology is to describe the evolution of the universe as a whole; our endeavour in this regard is through Einstein's theory of General Relativity. Spacetime is a 3+1 dimensional manifold armed with a Lorentzian metric, the intrinsic curvature of which manifests as gravity. The relation between curvature and its source (matter and energy) is governed *locally* by the Einstein Field Equations (EFEs) (1.1), which is a system of coupled, second order non-linear differential equations of the metric tensor:

$$G_{\mu\nu} \equiv R_{\mu\nu} - \frac{1}{2} R g_{\mu\nu} = 8\pi G T_{\mu\nu}. \tag{1.1}$$

The left hand side of the EFEs is *geometric*, in that it is a measure of curvature, while the right hand side is the *source* term, consisting of the Energy-Momentum tensor multiplied by a prefactor that ensures Bohr's correspondence principle in the Newtonian limit. All metrics in the thesis will maintain a $(-,+,+,+)$ convention.

Curvature: the Riemann, Ricci and Weyl tensors

Intrinsic curvature in a manifold results in an ambiguity in the comparison of vectors and tensors at different points. The transport of a vector from one point to another is path dependent; the extent to which a vector changes in a simple closed path from a point to itself is captured by the **Riemann tensor**, and this serves as a measure of intrinsic curvature.

Mathematically it is computed as the deviation from commutativity of two covariant derivatives. When working with torsion-free, metric compatible (Christoffel) connections, the Riemann tensor is given by:

$$R^{\rho}{}_{\sigma\mu\nu} = \partial_{\mu}\Gamma^{\rho}{}_{\nu\sigma} - \partial_{\nu}\Gamma^{\rho}{}_{\mu\sigma} + \Gamma^{\rho}{}_{\mu\lambda}\Gamma^{\lambda}{}_{\upsilon\sigma} - \Gamma^{\rho}{}_{\nu\lambda}\Gamma^{\lambda}{}_{\mu\sigma}. \tag{1.2}$$

The Riemann tensor with a lowered index ($R_{\rho\sigma\mu\nu}$) is antisymmetric under $\rho \leftrightarrow \sigma$ and $\mu \leftrightarrow \nu$, symmetric under $\rho\sigma \leftrightarrow \mu\nu$, and has a vanishing cyclic permutation on the last three indices. The number of independent components of the Riemann tensor in light of these symmetries is given by $\frac{1}{12}n^2(n^2-1)$ where n is the dimensionality of the space. In 3+1 dimensional space, the Riemann tensor has 20 independent components.

Analogous to a rank-two tensor being split into a trace and trace-free component, the rank-four Riemann tensor is split into a 2-index 'trace' (**Ricci tensor** and Ricci scalar) and a 4-index 'trace-free' (**Weyl tensor**) part. The contraction of the Riemann tensor is achieved uniquely with the Christoffel connection, and the Ricci tensor is then given by:

$$R_{\mu\nu} = R^{\lambda}{}_{\mu\lambda\nu}. \tag{1.3}$$

The trace of the Ricci tensor is the Ricci scalar. Together, these two terms contain all information about contractions of the Riemann tensor. The Weyl tensor captures all the trace-free parts of the Riemann tensor, while still obeying its symmetries. Physically, the Ricci tensor measures the change in volume of a space (relative to Minkowski) due to intrinsic curvature, while the Weyl tensor is a measure of the volume-preserving distortions (shear and rotations) due to intrinsic curvature.

An interesting point to note is that while the 20-component Riemann tensor fully specifies intrinsic curvature, the source in the EFEs govern only 10 — the Ricci tensor component — of it. That begs the question of whether the Weyl tensor remains unspecified, and whether the intrinsic curvature (and hence gravity) is fully specified. Indeed that isn't the case; however, the Weyl tensor to GR is what electromagnetic radiation is to the theory of electrodynamics. Much like how Maxwell's equations with a source and appropriate boundary conditions can only specify the electric field in the region up to freely propagating electromagnetic radiation, the curvature of spacetime is specified by the EFEs up to the existence of gravitational

radiation as specified by the Weyl tensor.

1.2 3 + 1 Covariant Formalism

The theory of General Relativity is *diffeomorphism invariant*, which is a high-brow way of saying that GR (unlike Newtonian gravity) is free of prior geometry. The metric (and hence the connection and volume element) appear in the field equations dynamically, and there is no geometry given to us ahead of time on which a preferred set of coordinates might be chosen. However, the symmetries of the system usually render the use of a particular set of coordinates useful by making the field equations more tractable.

Cosmological systems are usually described with respect to a set of well-behaved[1] observers whose time is assumed to measure the cosmic time. The world lines of the observers *thread* spacetime, and it is convenient to express coordinates relative to these fundamental world lines. *Generalized bases* of the vector spaces $T_p(M)$ at a point offer alternatives to the conventional coordinate basis, and have the advantage of being adapted to the system being studied by representing preferred velocities and observers. In a spacetime, such a basis is called a *tetrad*. In order to specify a tetrad with respect to the world lines generated by the fundamental velocity fields u^a, we split our 4-dimensional spacetime into a 3-dimensional spacelike hypersurface perpendicular to u^a and a timelike direction along u^a (since they are timelike vectors). The hypersurface then defines the space of observables for each of these observers. This is in practice achieved by:

1. Choosing a 3-dimensional surface S that intersects every world line exactly once, and labelling each world line at its intersection in S with 3 coordinates y^i.

2. Maintaining the same label for the world lines even after leaving the surface S. These constitute *comoving coordinates*.

3. Defining a time coordinate along the fundamental world lines that increase monotonically along their flow.

Such a choice of hypersurface might not always be possible; we require the 'vorticity' of the world lines to vanish, as will be discussed later. In the event of such a possibility, the tetrad (t, y^i) represent comoving coordinates adapted to the fundamental world lines. The choice

[1] see subsection (1.2.3)

of the initial surface S and time coordinate are not unique. As a result, the constant time hypersurfaces need not be locally orthogonal to every fundamental world line. There are classes of transformations that preserve the comoving form of coordinates; they correspond to changing the initial choice of constant time hypersurface ($t' = t'(t, y^i),\ y^{i'} = y^i$) or changing the labeling of world lines on the given hypersurface ($t' = t,\ y^{i'} = y^{i'}(y^i)$). The first transformation corresponds to 'tilting' the hypersurface with respect to the fundamental world lines while still satisfying condition (1) above, while the second transformation involves retaining the orientation of the hypersurface and relabeling the points.

A particularly useful choice of time coordinate is the proper time τ as measured along each fundamental world line. If we take s_0 to denote the time on the initial surface S, then $s = s_0 + \tau$ is called the *normalized time* and the coordinates are then *normalized coordinates*. Having fixed the time coordinate, the only freedom left to us is to choose the initial surface S, which is achieved by $s' = s + f(y^i)$. The choice of comoving coordinates is equivalent to the choice of Lagrangian coordinates in fluid mechanics; fixed coordinates similar to Eulerian coordinates may be constructed as well.

Coordinates adapted to preferred matter motion implies a preferred 4-velocity at each point. In the local coordinate basis x^μ (as opposed to y^i) measured in proper time, the preferred 4-velocity is a normalized timelike vector:

$$u^\mu = \frac{dx^\mu}{d\tau};\ \ u_\mu u^\mu = -1. \tag{1.4}$$

In normalized coordinates (s, y^i), we have:

$$u^\mu = \delta^\mu_0;\ \ \frac{ds}{d\tau} = 1,\ \frac{dy^i}{d\tau} = 0. \tag{1.5}$$

1.2.1 Some useful definitions:

The following formulae are motivated rigorously in [EMM12], and are summarized here for completeness.

Projection tensors:

In order to achieve projection parallel and perpendicular to u^a, we need to define projection

tensors. This is done by constructing the tensor operators $U^a{}_b$ and h_{ab}, respectively, as:

$$\begin{aligned} U^a{}_b &:= -u^a u_b, \\ h_{ab} &= g_{ab} + u_a u_b, \end{aligned} \tag{1.6}$$

with the obvious contractions:

$$\begin{aligned} &U^a{}_b U^b{}_c = U^a{}_c, \quad U^a{}_a = 1, \quad U^a{}_b u^b = u^a; \\ &h^a{}_b h^b{}_c = h^a{}_c; \quad h^a{}_a = 3; \quad h^a{}_b u^b = 0. \end{aligned} \tag{1.7}$$

Here, g_{ab} is the local 3+1 D metric for a particular world line. The tensor projection along u^a can be used to define the time derivative of a tensor along the fluid flow lines:

$$\dot{S}^{a\cdots}{}_{b\ldots} = u^c \nabla_c S^{a\cdots}{}_{b\ldots} = \frac{\mathrm{d}}{\mathrm{d}\tau} S^{a\cdots}{}_{b\ldots} + S^{c\cdots}{}_{b\ldots} \Gamma^a_{cd} u^d + \cdots - S^{a\cdots}{}_{c\ldots} \Gamma^c_{bd} u^d - \cdots . \tag{1.8}$$

This amounts to a usual directional derivative with respect to the proper time τ with the requisite correction terms to make the derivative covariant. In particular, the acceleration vector is given by:

$$\dot{u}^a = u^b \nabla_b u^a \Rightarrow \dot{u}^a u_a = 0, \tag{1.9}$$

which vanishes *iff* the flow lines are geodesic, which is usually the case when the observers move under the influence of gravity alone in the absence of other forces such as viscosity.

The orthogonal projection tensor h_{ab} is interpreted as the instantaneous rest frame for each observer at a point and hence defines local surfaces of simultaneity. It is also the metric tensor for the instantaneous rest space of the observers; it serves to define distances and inner products:

$$X^a u_a = 0 = Y^b u_b \Rightarrow \mathbf{X} \cdot \mathbf{Y} = X^a g_{ab} Y^b = X^a h_{ab} Y^b. \tag{1.10}$$

Finally, the Projected Symmetric Trace-Free parts (PTSF) of tensors are obtained from the orthogonal projection tensor as:

$$V_{\langle a\rangle} = h^b{}_a V_b, \quad S_{\langle ab\rangle} = \left\{ h^c{}_{(a} h^d{}_{b)} - \frac{1}{3} h_{ab} h^{cd} \right\} S_{cd}. \tag{1.11}$$

Since our coordinates are adapted to the world lines of fundamental observers, the kinematics of these fundamental world lines would describe the expansions and distortions of the space-like hypersurface of simultaneity. In order to study this, we must first define 3-dimensional derivative operators that project onto the hypersurface orthogonal to observers:

$$\overline{\nabla}_c S^{a\cdots}{}_{b\cdots} = h_c{}^f h^a{}_d \cdots h_b{}^e \cdots \nabla_f S^{d\cdots}{}_{e\cdots}, \tag{1.12}$$

where each of the indices have been projected by an orthogonal projection tensor of their own. From this we can define:

$$\begin{aligned} &\operatorname{div} V = \overline{\nabla}^a V_a, \quad (\operatorname{div} S)_a = \overline{\nabla}^b S_{ab}; \\ &\operatorname{curl} V_a = \eta_{abc} \overline{\nabla}^b V^c, \quad \operatorname{curl} S_{ab} = \eta_{cd(a} \overline{\nabla}^c S_{b)}{}^d. \end{aligned} \tag{1.13}$$

In general, these are operators only in the tangent hyperplane at each point and not necessarily in all of the 3-dimensional manifold. The latter holds only when the 'vorticity' of the fundamental velocity vanishes.

From these definitions, the covariant derivative of the fundamental 4-velocity itself can be split as:

$$\nabla_b u_a = h_a{}^c h_b{}^d \nabla_d u_c + U_a{}^c U_b{}^d \nabla_d u_c = \overline{\nabla}_b u_a - \dot{u}_a u_b. \tag{1.14}$$

1.2.2 Deriving a generalized Hubble law

With all the artillery developed so far, we can define relative positions and velocities on the hypersurface.

In comoving coordinates (s, y^i) consider a curve $y^i = y^i(v)$ on the surface $S(s = s_0)$ that links a set of fundamental world lines on S. Since the coordinates are comoving, the curve will continue to link the same fundamental world lines at later times as well. The curve $y^i(v)$ is dragged along in time by the world lines. The tangent vector to the curve $\beta^a = (0, \delta y^i) = (0, \frac{dy^i}{dv}\delta v)$ will be similarly dragged, and will hence always connect the same pair of world

lines. These tangents are hence called *connecting vectors*. This means an observer O will at see the displacement vector β^a point to the *same* galaxy's world line *at all times*.

Now, what we want is a displacement which represents an instantaneous spatial displacement as measured in O's rest frame, and so is orthogonal to the u^a. The displacement we have is not always orthogonal to the fluid flow lines; it may contain an incremental time displacement as well, depending on the surface $S(s = s_0)$. The requisite displacement is obtained by projecting β^a orthogonal to u^a, i.e., by taking its PTSF part. So, the relative position vector in the instantaneous rest frame of the observer O is given by:

$$\beta^{\langle a\rangle} = \delta l e^a \tag{1.15}$$

where δl is the magnitude or distance, and e^a the unit direction vectors in the instantaneous rest frame of O obeying:

$$e^a e_a = 1, \quad e^a u_a = 0 \Rightarrow \beta^{\langle a\rangle}\beta_{\langle a\rangle} = (\delta l)^2. \tag{1.16}$$

The relative velocity vector is obtained by first taking the time derivative of the PTSF connecting vector, and then projecting this derivative orthogonal to u^a. So:

$$v^a = v^{\langle a\rangle} = h^a{}_b u^d \nabla_d \left(h^b{}_c \beta^c\right) = \dot{\beta}^{\langle a\rangle}. \tag{1.17}$$

Since the vector β^a is dragged along by the fundamental 4-velocities, its Lie bracket with u^a vanishes. This gives us:

$$[\boldsymbol{u}, \boldsymbol{\beta}]^a = u^a{}_{,b}\beta^b - \beta^a{}_{,b}u^b = 0 \Rightarrow \beta^b \nabla_b u^a = u^b \nabla_b \beta^a. \tag{1.18}$$

Substituting this relation in eq. (1.17) gives:

$$v^a = V^a{}_b \beta^{\langle b\rangle}, \tag{1.19}$$

where

$$V_{ab} := h_a{}^c h_b{}^d \nabla_d u_c = \overline{\nabla}_b u_a. \tag{1.20}$$

The formula in eq. (1.19) is reminiscent of Hubble's law, indeed, it may be interpreted as a generalized Hubble law!

The covariant derivative of the fundamental 4-velocity can be used to study the kinematics of the relative position. This is done by splitting the projected covariant derivative of u^a into its irreducible parts under rotations. Since V_{ab} is a rank two tensor, it can first be split as a symmetric and anti-symmetric part. The symmetric part can further be split as a trace and trace-free component.

$$V_{ab} = V_{(ab)} + V_{[ab]} = \Theta_{ab} + \omega_{ab} = \Theta_{\langle ab\rangle} + \frac{1}{3}\Theta^c{}_c h_{ab} + \omega_{ab} \equiv \sigma_{ab} + \frac{1}{3}\Theta h_{ab} + \omega_{ab}. \tag{1.21}$$

So:

$$V_{ab} = \frac{1}{3}\Theta h_{ab} + \sigma_{ab} + \omega_{ab}. \tag{1.22}$$

Before understanding the individual physical relevance of the terms, we can, from equations (1.19) and (1.20), derive an explicit generalized Hubble law:

$$\frac{\dot{\delta l}}{\delta l} = \Theta_{ab} e^a e^b = \frac{1}{3}\Theta + \sigma_{ab} e^a e^b, \tag{1.23}$$

$$\dot{e}_{\langle a\rangle} = \omega_{ab} e^b + \sigma_{ab} e^b - \left(\sigma_{cd} e^c e^d\right) e_a. \tag{1.24}$$

The first equation tells us that the rate of distance is directly proportional to the magnitude of the distance; the constant of proportionality is in general dependent on the direction due to a shear (σ_{ab}) contribution (explained below). The second equation is the rate of change of direction as measured with respect to a non-rotating local inertial reference frame, determined by local dynamical experiments. Both the above equations are observable directly. The derivation will be correct provided the continuum (fluid) approximation is a good description of the matter distribution and velocities in the universe. In order to understand

the physics of the individual contributions, consider setting them to zero pairwise.

The case $\omega_{ab} = 0 = \sigma_{ab}$ is one of **pure expansion**, since the rate of change of relative distance becomes $\frac{\dot{\delta l}}{\delta l} = \frac{\Theta}{3}$ (independent of direction), while the rate of change of direction becomes zero. Hence we have a distortion-free expansion without any rotation.

Setting $\omega_{ab} = 0 = \Theta$ corresponds to **pure shear**. Since the shear tensor is symmetric and trace-free, we can choose an orthonormal basis of shear eigenvectors in which it is diagonal with trace zero. A vanishing trace tells us that an expansion in any one direction will result in a contraction in at least one other direction. Hence we have a pure distortion, without rotation or change of volume.

Finally, $\sigma_{ab} = 0 = \Theta$ is the case of **pure vorticity**, since the rate of change of relative distance is zero and only the direction changes. Since this preserves all distances, it represents a pure rotation, without distortion or expansion.

In a general fluid flow, all these quantities will be non-zero, so a combination of effects will occur. However, there will always be two instantaneous fixed points in the sky, where the galaxy directions for a given celestial sphere of galaxies remain constant; this follows from the fixed point theorem for vector fields on the 2-sphere.

We can define:

$$H = \frac{\dot{\delta l}}{\delta l} = \frac{1}{3}\Theta, \tag{1.25}$$

which serves as a *generalized Hubble parameter*. The value at the present time is the *Hubble constant*.

Before we move to the important question of whether a global spacelike hypersurface can be defined at all, let us take a moment to appreciate what we have derived so far. All we have done is define a coordinate system adapted to a set of preferred observers, without yet assigning properties to these observers (fluid particles). Our ignorance of their dynamical interaction notwithstanding, it appears we have arrived at a generalized Hubble law! This is an artefact of our choice of coordinates; the comoving coordinates on the spacelike hypersurface do not represent physical distances. In order to do so, it becomes necessary to multiply all coordinates by a prefactor that in general will depend on both the time coordinate as

well as the position in comoving space. This was tacitly assumed in assigning a 'length' (δl) to the position vector β^a. By doing this, we are effectively separating the time dependent aspect of the distance from the distance itself, thus giving us a magnitude of velocity that is proportional to the magnitude of the physical distance.

1.2.3 Vorticity and cosmic time

To finally address the elephant in the room, we determine under what conditions a set of observers can have a common surface of simultaneity (and hence a cosmic time). Consider the following heuristic argument that illustrates a way in which a common hypersurface cannot be constructed.

Take two observers in a 2+1 dimensional space whose world lines form a double helix about some common axis. The perpendicular two dimensional surface defined *locally* at each point on an observers world line is their local surface of simultaneity. If the two observers are close enough, it is easy to see that the surface of simultaneity at an instant of time of one observer will intersect the surface of simultaneity of the observer at some other instant of time, leading to a surface of simultaneity that intersects itself. This is purely due to the fact that the two observers are 'rotating' about an axis; their surfaces of observables cannot be smoothly patched together. As long as this rotation vanishes, a shear or volume expansion cannot cause this effect. This idea can be formalized mathematically as follows.

The vorticity vector ω^a can be written as the curl of the fundamental 4-velocity ($\omega_a = -\frac{1}{2}\operatorname{curl} u_a$), and so a vanishing vorticity necessarily means that u_a can be written as the gradient of a scalar potential; in particular,

$$\omega_a = 0 \equiv \text{there exist functions} \quad (r,t) \quad \text{such that} \quad u_a = -rt_{,a}, \tag{1.26}$$

where the comma before the function t represents a gradient (the covariant derivative of a scalar reduces to the regular partial derivative). This means that u_a is orthogonal to the surfaces $t =$ constant. At each point the tangent plane orthogonal to u_a is spanned by h_{ab} , but in general these surface elements do not mesh together to form a surface in spacetime. The orthogonal tangent planes are instantaneous rest spaces for observers moving with 4-velocity u_a; these fit together coherently if and only if $\omega_a = 0$. This is the condition for the existence of a cosmic time for the fundamental observers. This allows fundamental observers

to synchronise their clocks.

The potential function t will not measure *proper time*; the time derivative of t with respect to τ is

$$\dot{t} = u^a \nabla_a t = u^a t_{,a} = -\frac{1}{r} u_a u^a = \frac{1}{r}. \tag{1.27}$$

This can be set to 1 if $r \sim r(t)$ (r is a function of time only), whence we may simply re-scale our time coordinate t. Physically, this corresponds to ensuring that u^a has zero vorticity and that the flow lines are geodesic. For example, the time coordinate in the FLRW universe is a fundamental cosmic time that measures proper time along each world line. The standard time coordinate in a Schwarzschild solution is a cosmic time for static observers, but does not measure proper time along their world lines because their acceleration is non-zero.

1.3 Cosmological Models

With just a set of coordinates and observers, we have arrived at a generalized expansion law. For the exact functional dependence of the velocity of expansion to distance, we need the time evolution of the scaling prefactor that relates the comoving distances to physical distances. This involves specifying the distribution and thermodynamic properties of the matter that fills the universe, and this entire process constitutes constructing a *cosmological model*.

A cosmological model consists of a spacetime with well-defined, physically realistic, matter and radiation content alongside a uniquely defined family of fundamental observers whose world lines are expanding away from each other in some universe domain, resulting in a well-defined set of observational predictions for that domain.

These models must first match the observations we have at present to some time domain in its evolution, and the predictions it makes must be on theoretically sound ground with observations that can physically be made. The Standard Model in Cosmology is the ΛCDM paradigm that makes use of the FRW metric with an assumption of dark matter and dark energy, both of which can be viewed as *ad hoc* solutions to the discrepancies of the Standard Model. The underlying principle of the ΛCDM model is that of *statistical* homogeneity

and isotropy, which is mathematically implemented as an *exact* homogeneity and isotropy. There are myriad cosmological models with analytic solutions that break this symmetry; these include models that break homogeneity and models that break isotropy while retaining homogeneity. The exact details of these models can be found in most modern textbooks of relativistic cosmology; the interested reader may look at Relativistic Cosmology by George F.R. Ellis et. al. ([EMM12]) for a detailed review. This thesis considers the most general possible model that breaks both homogeneity and isotropy, as developed by Thomas Buchert et. al. ([BR12], [BC08] and references therein).

Chapter 2

The FRW Universe

2.1 The metric

Solutions to the EFEs are usually inferred through the symmetries of the problem; in cosmology the corresponding assumption is of statistical homogeneity and isotropy in the distribution of matter. Known as the *cosmological principle*, it is often stated as the existence of (fundamental) observers who see a homogeneous and isotropic universe, and whose time is taken to be the *cosmic time*. This translates to assuming a maximally symmetric space (not spacetime), which fixes the metric up to a dimensionless arbitrary function (the scale factor $a(t)$) and a constant (the curvature constant κ). The metric has the form:

$$ds^2 = -dt^2 + a(t)^2\gamma_{ij}dx^i dx^j = -dt^2 + a(t)^2\left(\frac{d\chi^2}{1-\kappa\chi^2} + \chi^2 d\Omega_2^2\right), \tag{2.1}$$

where γ_{ij} is a maximally symmetric spatial metric and $d\Omega_2^2 = d\theta^2 + sin^2\theta d\phi^2$ is the metric of a 2-sphere. The metric is called the Friedmann-Robertson-Walker (FRW) metric, and is written in units of $c = 1$. The curvature constant κ takes values in the domain of Real numbers; negative, vanishing and positive values representing hyperbolic, flat and spherical space, respectively. It is important to note that the Einstein equations are *local*, and so the metric is valid only at a point and does not dictate global curvature. The latter is inferred and restricted by the requirement of maximal symmetry in space.

The FRW metric is expressed in comoving coordinates χ, and so physical distances r are given by $r(t) = a(t)\chi$. From the metric and this relation alone, we can infer the Hubble expansion law $v(t) = \frac{\dot{a}}{a}r(t) := H(t)r(t)$, where $H(t)$ is the Hubble parameter that is a constant at

every instant of time. The velocity is hence proportional to the physical distance; the exact functional dependence requires knowledge of $a(t)$. It is important to note that this is not a physical velocity, in that it is not the velocity as perceived by an observer locally. This is the 'velocity' imparted to the fluid element that is stitched to space through comoving coordinates. Notice also, that owing to the high degree of symmetry (the highest possible on space, in fact), the scale factor $a(t)$ describes both the local distances and velocities, as well as their global counterpart. This is a point we will address again in Chapter (3).

2.2 The Friedmann Equations

Substituting the above metric in the EFEs, with a reasonable assumption of source, will yield evolution equations for the scale factor $a(t)$ in terms of the curvature constant κ. In the comoving frame of fundamental observers, a convenient choice of source is that of an ideal fluid with energy density ρ, isotropic pressure p and equation of state of the form $p = \omega\rho$. The proportionality constant ω can be interpreted as the enthalpy of the fluid if the flow is isentropic, as is usually the case[1]. The Energy-Momentum tensor $T_{\mu\nu}$ is then $diag(\rho, p, p, p)$ and the equations of motion for $a(t)$ are[2]:

$$3\frac{\ddot{a}}{a} = -4\pi G(\rho + 3p), \tag{2.2}$$

$$3\left(\frac{\dot{a}}{a}\right)^2 = 8\pi G\rho - \frac{3\kappa}{a^2}. \tag{2.3}$$

Equation (2.2) is known in literature as the Raychaudhuri equation, and eq. (2.3) the Hamiltonian constraint. A few interesting observations are that the curvature constant does not appear in the former, while the pressure does not influence the Hubble parameter as in the latter. This is closely related to the point made in footnote 2 and references therein.

There is an interesting question to be asked at this junction. Given any arbitrary metric

[1]For a general flow, we have $d\omega = TdS + (1/\rho)dP$, where $1/\rho$ is the specific volume. Setting dS to zero gives us our equation of state. Note that this requires only the lesser condition of an *adiabatic* flow; an isentropic flow is a more strict condition.

[2]The astute reader might recognise that the first equation is nothing but the Newtonian force law (if $p = 0$), while the second is a first integral of motion corresponding to Energy conservation if the curvature term were imparted an interpretation of total energy. This is indeed the case, and there has been a long-standing debate on the relevance of Newtonian relativity in cosmology. See [Mil00], [MM00] and [Nor92]

$g_{\mu\nu}$, can we solve the EFEs in reverse to find the matter distribution? Put differently, can we always find a suitable matter distribution to effect a curvature of our choice? A blind substitution to the left hand side of the EFEs would seem to suggest so. However, the corresponding stress-energy tensor obtained may not be one that is physically realisable in our universe. In order to preserve physicality, we are required to impose conditions on the stress-energy tensor by hand. Most such *energy conditions* boil down to a generalization of the idea that the energy density as observed by a timelike (or null) vector must be non-negative. The energy density is just the T_{00} term, but conditions on all the components of $T_{\mu\nu}$ correspond to imposing additional requirements on pressure, for example. The exact energy condition that our universe satisfies is yet to be known, but for our purposes, we would like to impose the condition that 'matter gravitates towards matter'. Referred to as the *Strong Energy Condition*, it stipulates that for every timelike vector field $\vec{X}$, the trace of the tidal tensor[3] measured by the corresponding observers is always non-negative:

$$\left(T_{ab} - \frac{1}{2}T g_{ab}\right) X^a X^b \geq 0. \tag{2.4}$$

For our particular stress-energy tensor, this condition boils down to $\rho + p \geq 0, \quad \rho + 3p \geq 0$. The consequence of this condition is that the acceleration of the scale factor (eq. 2.2) is always negative, meaning that if the universe is initially given a positive 'velocity' $\dot{a}$ initially, it evolves in a decelerating fashion. It is occasionally useful to speak in terms of Hubble parameters $H = \frac{\dot{a}}{a}$ and dimensionless deceleration parameters $q = -\frac{1}{H^2}\frac{\ddot{a}}{a}$. So, the strong energy condition insists that $q > 0$.

Observations, however, indicate that the universe is currently expanding at an accelerated rate. To reconcile with this discrepancy, the consensus is to include a positive Λ term to the right hand side of the two equations. Noting that the EFEs (1.1) depend on the stress-energy tensor and not its derivatives, we see that gravity sees the absolute value of energy, and not just a difference in energies. We therefore are at liberty to fix a ground state energy. Interpreting the cosmological constant Λ as a vacuum energy is tantamount to adding a $\Lambda g_{\mu\nu}$ term to the left hand side of the EFEs. This corresponds to modifying the Einstein Hilbert action R. Alternatively, we could have subtracted the same term from the right hand side of the EFEs, in which case the cosmological constant is interpreted as a *dark energy* with

[3]The tidal tensor represents the relative acceleration due to gravity of two test masses separated by an infinitesimal distance.

equation of state $p = -\rho$. The effect of such an inclusion is identical in either case, and the interpretations therefore have no physical distinctions through observation. The inclusion of such a term in the EFEs results in the Lemaitre equations, which are identical to the Friedmann equations but for an additional Λ term:

$$\begin{aligned} 3\frac{\ddot{a}}{a} &= -4\pi G(\rho + 3p) + \Lambda, \\ 3\left(\frac{\dot{a}}{a}\right)^2 &= 8\pi G\rho - \frac{3\kappa}{a^2} + \Lambda. \end{aligned} \tag{2.5}$$

The first of the above equations now allows for an acceleration if Λ is sufficiently large. Since we are dealing with fluids, we additionally require an energy continuity (conservation) equation:

$$\dot{\rho} = 3\frac{\dot{a}}{a}(\rho + p). \tag{2.6}$$

This equation is readily obtained from taking the 0-0 component of the covariant derivative of the stress-energy tensor upon substituting the metric (2.1). Equations (2.5) and (2.6) govern the dynamics of the scale factor, and constitute the Standard Model.

2.3 3+1 Split for the FRW Universe

The assumption made in arriving at the FRW metric was of *statistical* homogeneity and isotropy, which stipulates that at the largest scales, the universe can be represented by averaged quantities that are invariant under translation or rotation beyond a homogeneity scale. In practice, this was implemented as an *exact* homogeneity and isotropy. In the jargon of formalism developed in Chapter 1, this assumption would correspond to a set of fundamental observers whose world lines had no shear and vorticity. This would result in a convenient foliation of spacetime in which maximally symmetric spacelike hypersurfaces can be stacked up congruently, with a cosmic time parameter that is *always* orthonormal to the hypersurfaces. Each observer would measure the same cosmic time coordinate in such a foliation; this will not coincide with the epoch assigned by an observer to a particular event. Maximal symmetry will ensure, however, that if one observer assigns an epoch to the observation of another observer, the second observer will assign the same epoch to the first.

Before presenting the Friedmann equations in a covariant fashion, it helps to know what we are doing differently here. There are two ways to decompose and solve the EFEs (and fix coordinates in a 3+1 dimensional spacetime); we can either use the symmetries of the system to foliate our spacetime into hypersurfaces on which we fix a metric, or we can thread our spacetime with fundamental trajectories and define a set of coordinates adapted to them. These are then used to define locally orthogonal hypersurfaces that must be smoothly patched together. The two approaches should ultimately lead to the same physics for a given system.

In order to effect the latter approach, we begin by projecting the stress-energy tensor orthogonal to the worldlines as:

$$T_{\alpha\beta} = \rho u_\alpha u_\beta + q_\alpha u_\beta + q_\beta u_\alpha + p h_{\alpha\beta} + \pi_{\alpha\beta}, \tag{2.7}$$

where $\rho = T_{\alpha\beta}u^\alpha u^\beta$ is the total energy density, $p = \frac{1}{3}T_{\alpha\beta}h^{\alpha\beta}$ is the isotropic pressure, $\pi_{\alpha\beta} = T_{\gamma\delta}h^\gamma{}_{\langle\alpha}h^\delta{}_{\beta\rangle}$ is the anisotropic stress, and $q_\alpha = -T_{\gamma\beta}u^\beta h^{\gamma\alpha}$ is the relativistic momentum density. These satisfy the properties:

$$\pi_{\alpha\beta} = \pi_{(\alpha\beta)}, \quad \pi^\alpha{}_\alpha = 0, \quad \pi_{\alpha\beta}u^\alpha = 0. \tag{2.8}$$

The relativistic momentum density is spacelike, meaning $q_\alpha u^\alpha = 0$.

The evolution of spacetime can now be obtained from the definition of the Riemann tensor that makes use of vectors: $2\nabla_{[\alpha}\nabla_{\beta]}u^\gamma = R^\gamma{}_{\alpha\beta\delta}u^\delta$, and the twice contracted Bianchi identity on the Riemann tensor: $\nabla_\alpha R^\alpha{}_\beta = \frac{1}{2}\nabla_\beta R$. This decomposes the left hand side of the EFEs. The resultant equations are obtained by projection and equating to the stress-energy tensor; the equations can be split as scalar, vector and tensors based on their transformation under rotation. The scalar equations[4] read:

$$\begin{aligned}
&\dot{\Theta} + \frac{1}{3}\Theta^2 = -4\pi G(\rho + 3p) - 2\sigma^2 + 2\omega^2 + \nabla_\alpha \dot{u}^\alpha + \dot{u}^\alpha \dot{u}_\alpha + \Lambda, \\
&\frac{1}{3}\Theta^2 = 8\pi G\rho - \frac{1}{2}{}^{(3)}R + \sigma^2 - \omega^2 + \Lambda, \\
&\dot{\rho} + \Theta(\rho + p) = -\nabla^\alpha q_\alpha - 2\dot{u}_\alpha q_\alpha - \sigma_{\alpha\beta}\pi^{\alpha\beta}.
\end{aligned} \tag{2.9}$$

[4] To see the projection in all its tensor glory, read [Mag12]. Masochists who wish to derive these equations rigorously may find helpful tricks in [EMM12], and for a complete derivation may contact the author of this thesis.

When considering an *ideal* fluid, we put the anisotropic stress to zero; the relativistic momentum density vanishes in the local rest frame of the observers. This leaves us with the total energy density and isotropic pressure. The equations now read:

$$\begin{aligned}
&\dot{\Theta} + \frac{1}{3}\Theta^2 = -4\pi G_{\mathrm{N}}\rho - 2\sigma^2 + 2\omega^2 + \Lambda, \\
&\frac{1}{3}\Theta^2 = 8\pi G_{\mathrm{N}}\rho - \frac{1}{2}{}^{(3)}R + \sigma^2 - \omega^2 + \Lambda, \\
&\dot{\rho} + \Theta\rho = 0.
\end{aligned} \tag{2.10}$$

While homogeneity and isotropy would also require the shear and vorticity terms to go to zero, we leave them in the equations until the very end for generality. However, in their absence, it is clear that the first two equations above are generalizations of the Friedmann equations, while the third is the continuity equation. These equations are *local*, since the projection tensors employed pertain to the local surface of simultaneity of a particular observer. In the absence of vorticity, we can smoothly patch these surfaces together on which the original Friedmann equations hold. We have thus obtained the same physics, but using a different approach to coordinates. This approach has the benefit of being covariant, since we are performing all contractions using projection operators that make use of vector fields.

Chapter 3

Inhomogeneous Cosmologies

At the heart of the discrepancy observed on the sign of q in section (2.2) is *potentially* the fact that a statistical cosmological principle is being implemented as an exact, local symmetry. The EFEs are manifestly non-linear equations; it is fair to suppose that the process of evolving quantities (like the densities, scale factors etc) in time should not commute with averaging them over a spacelike hypersurface at some instant of time. Put more explicitly, the time evolution of an average quantity should not display the same dynamics as explicitly evolving each local quantity in time, and then at every instant asking what its average value is. The FRW formalism evidently takes the former approach; the density is assumed to have the same value at every point and every length scale, and the Friedmann equations (2.5) model the evolution of these average quantities. The scale factor is assumed to depict the dynamics of both the local as well as global hypersurface. In the presence of such symmetry, the commutator of the two operations vanishes trivially[1].

The deviation from this exact homogeneity and isotropy and structure formation is traditionally effected via linear perturbations to the FRW metric. This corresponds to the regime in which the deviation of the density from its average value (often referred to as the *density contrast*; $\delta := \frac{\rho}{\bar{\rho}} - 1$) is lesser than unity. A detailed and very insightful review of the subject can be found in [MFB92]. The key point to note is that for $\delta < 1$, the perturbations decouple from the dynamics of the scale factor on average, *by construction*. Therefore, the non-commutativity mentioned above makes no appearance here.

The formation of non-linear structures ($\delta \gtrsim 1$) is modelled numerically via either one of

[1] See discussion after equation 3.7

Newtonian mechanics or N-body simulations. In both approaches, an underlying, tacit assumption is made on the validity of the ΛCDM paradigm in choosing a cosmic time, and the interactions that are imposed identically on each individual region or particle. The Buchert formalism summarized below makes no such assumption, and gives the problem a most general treatment from the linear regime itself. Idealizations that are expedient for the formulation of toy models are explicitly stated and imposed only at the very end. This model is not without its drawbacks; these (somewhat debilitating) shortcomings are discussed in detail at the end of the chapter.

3.1 Introduction to the Buchert Formalism

In order to model inhomogeneities in all their glory, we must work with the covariant formalism developed in section (1.2). Under this paradigm, we have already obtained the local dynamical equations for a cosmological system (eq. (2.10)). This makes no reference to the cosmological principle; and no symmetries have been imposed except for a vanishing momentum density and viscosity (ideal fluid in its local rest frame). To compute the value of the averages at each instant of time, we must define a consistent *averaging procedure*. The one outlined below was introduced by Buchert et. al. ([BR12]).

We must now enforce the additional constraint that the individual observers have a vanishing vorticity at every instant of time in order to meaningfully develop an averaging procedure on each spacelike hypersurface. This assumption, while absolutely necessary for the formalism, is also one of its most serious drawbacks: vorticity is the predominant stabilizing force in collapsing structures; virialization is achieved in galaxies and other clusters only in the presence of angular perturbations. We shall, nevertheless, proceed to see where this formalism takes us.

3.1.1 Averaging procedure

Consider a foliation of spacetime into spacelike hypersurfaces that have been constructed to be locally orthogonal to each observer. The average value of a scalar field f on this foliation can then be defined as:

$$\langle f \rangle(t) := \frac{\int_t f\varepsilon}{\int_t \varepsilon}, \tag{3.1}$$

where

$$\varepsilon := \sqrt{|^{(3)}g|}dx^1 \wedge dx^2 \wedge dx^3 \tag{3.2}$$

is the volume element on the hypersurface, and $\int_t \varepsilon$ is the volume of some domain in the hypersurface at time t. The scale factor can immediately be defined by:

$$a(t) := \left(\frac{\int_t \varepsilon}{\int_{t_0} \varepsilon}\right)^{1/3}, \tag{3.3}$$

or the cube root of the volume at time t, normalized by the volume at some initial origin of time. Since the left hand side of the Friedmann equations are kinematic, we first perform an average of the volume expansion term Θ:

$$\langle\Theta\rangle(t) \doteq \frac{\int_t \Theta\varepsilon}{\int_t \varepsilon} = \frac{\partial_t \int_t \varepsilon}{\int_t \varepsilon} = 3\frac{\dot{a}}{a}. \tag{3.4}$$

In going from the second to the third expression, we make use of the fact that we're using comoving coordinates adapted to our fundamental four-velocities. The derivation is summarized here for completeness. The volume expansion is the trace of the covariant derivative of the fundamental velocity: $\Theta = \nabla_\alpha u^\alpha = \partial_\alpha u^\alpha + \Gamma^\alpha_{\alpha\beta}u^\beta$. Since we are in the local rest frame of our observers, the only non-zero component of the four-velocity is the time-component, which has a value of c. Thus, the partial derivative term vanishes identically. In units of $c = 1$, the second term is simply $\Gamma^\alpha_{\alpha 0}$. Generally, the once 'contracted' Christoffel can be expressed as:

$$\Gamma^\alpha_{\alpha\beta} = \frac{1}{2}g^{\alpha\mu}(\partial_\alpha g_{\mu\beta} + \partial_\beta g_{\alpha\mu} - \partial_\mu g_{\alpha\beta}) = \frac{1}{2}g^{\alpha\mu}\partial_\beta g_{\alpha\mu} = \frac{1}{2}\operatorname{tr}(g^{-1}\partial_\beta g). \tag{3.5}$$

The last equality follows from the definition of trace for a symmetric matrix. In order to bring the trace into a more useful form, we make use of the identity: $\log(\det g) = \operatorname{tr}(\log g)$, which holds for *any* matrix g. A quick proof is seen easily for symmetric matrices like the metric: in its eigenbasis, g is diagonal, and $\log(g)$ has eigenvalues $\log(\lambda_i)$ if the matrix g has eigenvalues λ_i. Thus, $\operatorname{tr}(\log g) = \sum_i \log(\lambda_i) = \prod_i \lambda_i = \log(\det(g))$. Since the theorem

involved determinants and traces that are independent of basis, it holds true in general. The Christoffel hence reduces to $\Gamma^{\alpha}_{\alpha\beta} = \partial_\beta \log \sqrt{|\det g|}$.

Therefore, our expression for the volume expansion reduces to $\Theta = \partial_t \log \sqrt{|\det g|}$. Relating this to the measure that appears in the expression for the volume element (3.2) gives us the expression for the average volume expansion.

This mathematical digression aside, we have arrived at a nifty result! *The average volume expansion can be interpreted as an effective Hubble parameter for the domain that is being averaged over*. Before averaging the projected Friedmann equations, we must perform one final act of mathematical acrobatics: the spatial average of the time derivative of Θ, i.e., $\langle \dot{\Theta} \rangle$. We approach this in a more general fashion, to derive explicitly the extent of non-commutativity of time evolution and spatial averaging of a general scalar field f. Consider:

$$\begin{aligned} \partial_t \langle f \rangle &= \partial_t \frac{\int_t f\varepsilon}{\int_t \varepsilon} \\ &= \frac{\partial_t \int_t f\varepsilon}{\int_t \varepsilon} - \left(\frac{\int_t f\varepsilon}{\int_t \varepsilon}\right)\left(\frac{\partial_t \int_t \varepsilon}{\int_t \varepsilon}\right) \\ &= \frac{\int_t \partial_t(f)\varepsilon}{\int_t \varepsilon} + \frac{\int_t f \partial_t(\varepsilon)}{\int_t \varepsilon} - \langle f \rangle \langle \Theta \rangle \\ &= \langle \dot{f} \rangle + \langle f\Theta \rangle - \langle f \rangle \langle \Theta \rangle. \end{aligned} \tag{3.6}$$

Therefore,

$$\partial_t \langle f \rangle - \langle \dot{f} \rangle = \langle f\Theta \rangle - \langle f \rangle \langle \Theta \rangle. \tag{3.7}$$

The commutator of time evolution and spatial averaging of a scalar field f is therefore its covariance with the volume expansion. This is not surprising! The leading term first averages the scalar field at some instant of time, and asks how that average varies in time. This is the FRW paradigm. The second begins by finding the variation of f in time (on a particular spacelike hypersurface) at every point in space, and asks what its average value is. Since the average of f is defined relative to the volume element, it is not surprising that Θ (which in a way, measures the change in volume) appears on the right hand side. The change in the *average* value of f in time is due to two effects: the average of the change in f itself, as given by $\langle \dot{f} \rangle$, and the change due to the average volume of the spacelike hypersurface. The

latter is what decouples as a covariance. There are two ways in which the right hand side can vanish: firstly (and trivially), if $\Theta = 0$ identically, which corresponds to there being no volume expansion. This makes sense, for then the change in the average value of f is due only to the average change in f. The second way is for the fields f and Θ to be independent, making their covariance vanish non-trivially. This can happen in many ways, but in the specific case of the FRW paradigm, it is due to the maximal symmetry corresponding to a vanishing shear (and vorticity) everywhere. This makes the volume expansion rate constant, and hence the covariance above zero. For a general fundamental velocity field, however, the commutation is non-zero. The average of $\dot{\Theta}$ is then $\partial_t\langle\Theta\rangle - \mathrm{var}(\Theta)$.

3.1.2 3+1 Split under averaging

We now proceed to average eqs. (2.10), taken with Λ and ω set to 0. The equations obtained are[2]:

$$\begin{aligned} 3\frac{\ddot{a}}{a} &= -4\pi G_{\mathrm{N}}\langle\rho\rangle + \mathcal{Q}, \\ 3\left(\frac{\dot{a}}{a}\right)^2 &= 8\pi G_{\mathrm{N}}\langle\rho\rangle - \frac{1}{2}\left\langle {}^{(3)}R\right\rangle - \frac{1}{2}\mathcal{Q}, \\ \mathcal{Q} &\equiv \frac{2}{3}\left(\left\langle\Theta^2\right\rangle - \langle\Theta\rangle^2\right) - 2\left\langle\sigma^2\right\rangle. \end{aligned} \tag{3.8}$$

This is promising! Comparing the above equations with (2.10), we see that we have now obtained an additional term $\mathcal{Q}$, called the *backreaction*, in the Raychaudhuri equation. Notice that the backreaction term is expressed as the variance of Θ, a term that goes to zero along with the shear term, returning us to the FRW paradigm in the regime of high (and exact) symmetry. Also, the above equations hold across all regimes, linear or otherwise. The value of $\mathcal{Q}$ is small in the linear regime, and has a dominating effect only in the non-linear regime.

In light of these equations, we could hope that if the shear is small, and the variance in the volume expansion is *large enough*, then we may explain an accelerated expansion from the presence of inhomogeneities *alone*. Of course, we can always include the Λ term and share the cause of acceleration between them both. We shall, however, attempt to isolate the effect

[2]The averaging procedure is quite trivial when one substitutes for Θ in terms of the scale factor a as derived above; in order to find $\langle\dot{\Theta}\rangle$, we make use of the commutation rule. Again, a troubled reader may contact the author of the thesis for a detailed derivation.

of the former by setting Λ to zero, and ask how far inhomogeneities alone can take us.

The above equations are formidably intractable; we not only need to specify an inhomogeneous distribution of matter, but also explicitly construct our smoothly patched foliation to perform concrete averages and calculations. To simplify our problem and make any quantitative progress, we are forced to begin with absurdly pedestrian toy models. Unphysical as they seem, they go a long way in helping us isolate the various effects at play in the contribution of $\mathcal{Q}$.

Before that, however, there are few interesting conclusions we can draw from the general equations themselves. Notice that the Hamiltonian constraint above has a negative contribution from the backreaction, as opposed to the positive effect that Λ had. This means that the effect of inhomogeneities is to increase the acceleration, but reduce the value of the 'velocity', as measured by the square of the Hubble parameter. This potentially implies an upper bound on the value of the dimensionless Hubble parameter Ht; this is indeed the case, as has been shown in [Räs06b]. The paper also proves the existence of a lower bound on q, the dimensionless deceleration parameter. The arguments are summarized here for completeness.

The Raychaudhuri equation in the absence of vorticity (2.5) can be read as an inequality

$$\dot{\Theta} + \frac{1}{3}\Theta^2 \leq 0, \tag{3.9}$$

since the right hand side is always negative. The left hand side is essentially the projected local acceleration rate; so the local acceleration at every point in spacetime is non-positive. The averaged equation (3.8), however, has a backreaction term that allows the *average* acceleration to be positive. Recall that the origin of the positive backreaction term post averaging is the non-commutativity of time evolution and spatial averaging. More precisely, $\partial_t\langle\Theta\rangle = \langle\dot{\Theta}\rangle + \langle\Theta^2\rangle - \langle\Theta\rangle^2 > \langle\dot{\Theta}\rangle$. This can be interpreted as the growth in the volume of a hypersurface of constant time compensating for the decrease in the local expansion rate. Despite the acceleration now taking positive values, there will still be upper bounds on both Ht and q. The exact local Raychaudhuri equation can be viewed as an inequality (3.9) and integrated to give:

$$\frac{1}{\Theta(t,\mathbf{x})} - \frac{1}{\Theta(t_i,\mathbf{x})} \geq \frac{1}{3}(t - t_i), \tag{3.10}$$

where t_i is some initial time. Recall that Θ is the local volume expansion rate given by the tracing the covariant derivative of the fundamental 4-velocity. The volume expansion rate can be either positive, negative or zero; inequality (3.10) holds separately when it is positive and negative, but not when it passes through zero since it is not defined at that point. The intial time can be chosen as the Big Bang ($t_i = 0$), and the volume expansion rate at this origin $\Theta(t_i, \mathbf{x})$ taken positive instantaneously. This results in the upper bound:

$$\Theta(t,\mathbf{x}) \leq \frac{3}{t} \equiv \Theta_{max}(t). \tag{3.11}$$

A few remarks: (i) The inequality as suggested by the Raychaudhuri equation (3.9) holds true only for matter satisfying the strong energy condition ($\rho + 3p > 0$). (ii) The inequality is on the value of $\Theta(t,\mathbf{x})$, not on its absolute value. The upper bound (3.11) holds trivially for negative values of $\Theta(t,\mathbf{x})$ as well; this corresponds to the fact that the rate of collapse is not bounded from below. (iii) By assuming that the initial volume expansion rate is positive, we assume that the volume expansion rate is always positive, since we cannot afford Θ changing sign through zero. The upper bound is hence only for the expansion rate, and not for the rate of collapse. The collapse rate is not bounded from below, and can cause rapid change in Ht. In the actual simulation of the system, since the overdense are taken to virialize at half the radius of turnaround, the net Ht is bound by 1 from above. If not for virialization, q can become arbitrarily negative; it can diverge to negative infinity in finite time as well. (iv) The maximum value of $\Theta(t,\mathbf{x})$ depends only on the global time, and not on the position on the hypersurface of constant time. As a result, the (spatial) average value of $\Theta(t,\mathbf{x})$ is also bounded by the same number:

$$H \equiv \frac{1}{3}\langle\Theta\rangle \leq \frac{1}{3}\Theta_{max} = \frac{1}{t}. \tag{3.12}$$

The above relation gives us net the Hubble parameter in terms of the age of the universe. The above upper bound on the net Hubble parameter implies that the acceleration $\ddot{a}$ cannot be forever increasing; indeed, it cannot be a constant positive value for an arbitrarily long time either. It must asymptotically go to zero, become negative, or oscillate about zero or

some negative number. A more precise bound on the deceleration parameter can be obtained by considering the rearranged average Raychaudhuri equation[3] (3.23) as an inequality:

$$q \geq 2 - \frac{2}{9}\frac{\langle\Theta^2\rangle}{H^2} \geq 2 - \frac{2}{9}\frac{(\Theta_{max})^2}{H^2} = 2 - \frac{2}{(Ht)^2}. \tag{3.13}$$

Here, in going through the second inequality, we make use of (3.11). This holds only if Θ is nowhere negative; recall that the bound is not on the absolute value. Regions of negative Θ correspond to gravitational collapse, an intrinsically unstable process if not for virialization, at which point the above equations break down anyway. So, regions of collapse will have to be neglected in the estimate of lower bound for q.

To summarise [Räs06b], the dimensionless Hubble parameter is bounded above by 1 and the deceleration parameter can take arbitrarily negative values in the presence of gravitational collapse. It is interesting to see how this stacks up against the FLRW model constraints. In the FLRW model, Ht can grow without limit since dark energy violates the strong energy condition with $\omega = -1$. However, the deceleration parameter is bounded below by -1; $q < -1$ violates the null-energy condition.

The question naturally is if, in finding candidates for present time t_0 in a toy model, it is fair to simply equate the values of the Hubble parameter. The Hubble parameter is an observed (measured) quantity; and if the value of the observed (dimensionless) Hubble parameter is greater than 1, it is fair to suppose that the averaging formalism developed is not accurate. The possible values of H_0 from Type 1a Supernovae range between 55 and 75 km/sec/Mpc. Expressed in units of time inverse (Gyr^{-1}), H_0 ranges between 0.0562 and 0.0766[4].

One final remark is in order before we finally get to the toy models: What behaviour does this universe on average obey in terms of curvature? The observations today seem to indicate that the universe on average has zero curvature; is this predicted by the inhomogeneous universe as well? Without going into any detail[5], the answer is no; the averaging formalism suggests that the universe on average in the non-linear regime evolves like a universe with a slightly negative curvature. This is not a problem perse; the arguments made in the cited

[3] Sincere apologies for the causality-violating cross-referencing of equations; this particular rearrangement is, however, trivial.

[4] Phew!

[5] Readers interested in the details may look into [BC08].

review put Λ to zero, and so there is a modelling discrepancy in the way data is interpreted and fitted.

3.2 Toy Models

We now proceed to summarize the toy models that have already been constructed in literature ([Räs06a], [Räs08a]). The models are more elaborately motivated, justified and quantitatively studied than in the afore cited manuscripts. Their drawbacks are discussed, and a minor modification in the direction of generality is attempted in the next chapter.

3.2.1 2-region model

Formulation

This model was first introduced in [Räs06a]. The universe is considered a union of disjoint, spherically symmetric top-hat density perturbations about an EdS background. Disjoint implies that the spherical regions are isolated from each other (they do not share mass or come in contact at any point); the universe being a union of these perturbations means they aren't embedded in a 'background' universe: the universe *is* the set of spherical perturbations. The cosmic time parameter that determines the foliation is the time as measured by an observer in an EdS universe; we account for the explicit orientation of our foliation via an offset time, as will be elaborated on in section 3.2.1 and Appendix 6.

Isolation implies that the volumes are additive, and the Hubble parameter and deceleration parameter are calculated for the 2-region model as:

$$r = (r_1^3 + r_2^3)^{1/3}, \tag{3.14}$$

$$H = \frac{\dot{r}}{r} = \frac{r_1^3}{r_1^3 + r_2^3} H_1 + \frac{r_2^3}{r_1^3 + r_2^3} H_2 \equiv H_1(1 - v + vh), \tag{3.15}$$

$$q = -\frac{1}{H^2}\frac{\ddot{r}}{r} = q_1 \frac{1-v}{(1-v+hv)^2} + q_2 \frac{vh^2}{(1-v+hv)^2} - 2\frac{v(1-v)(1-h)^2}{(1-v+hv)^2}, \tag{3.16}$$

where $v = \frac{r_2^3}{r_1^3 + r_2^3}$ is the volume fraction of the overdense region, and $h = \frac{H_2}{H_1}$ is the Hubble parameter of the overdense region relative to the underdense one, and the additional term

at the end of (3.16) is the desired backreaction term; it relates directly to the backreaction term from the Buchert equations (derived explicitly later). These can be readily generalized for an n-region model as:

$$r = \left(\sum_i^n r_i^3 \right)^{1/3}, \tag{3.17}$$

$$H = \sum_i^n v_i H_i, \tag{3.18}$$

$$q = 2 + \frac{1}{H^2} \sum_i^n v_i H_i^2 (q_i - 2), \tag{3.19}$$

where

$$H_i = \frac{\dot{r}_i}{r_i}, \quad q_i = -\frac{1}{H_i^2} \frac{\ddot{r}_i}{r_i}, \quad v_i = \frac{r_i^3}{\sum_j^n r_j^3}$$

The above equations (3.17 - 3.19) reduce to (3.14 - 3.16) when $n = 2$. It remains to show how the backreaction term in the Buchert equations corresponds exactly to the additional term in the deceleration parameter above. Besides, the theoretical existence of a positive term does not imply that the specific implementation in the toy model is the same! The projected Friedmann equations for the FRW metric in the absence of vorticity read:

$$\begin{aligned} \dot{\Theta} + \frac{1}{3}\Theta^2 &= -\frac{\kappa^2}{2}\rho - 2\sigma^2, \\ \frac{1}{3}\Theta^2 &= \kappa^2 \rho - \frac{1}{2}{}^{(3)}R + \sigma^2, \end{aligned} \tag{3.20}$$

where $\kappa^2 = 8\pi G_{\mathrm{N}}$, G_{N} is the Newtonian Gravitational constant. The left hand side of the first equation of (3.20) is precisely $3\frac{\ddot{a}}{a}$, so we have

$$\frac{\ddot{a}}{a} = -\frac{1}{3}\left(\frac{\kappa^2}{2}\rho + 2\sigma^2 \right). \tag{3.21}$$

Since these equations have not been averaged yet, they hold in each of the individual spherical perturbations which evolve according to the spherical collapse model[6] (individual FRW

[6]See next subsection and Appendix 6 for a detailed exposition.

universes embedded in an EdS background). Now, averaging equations (3.20) gives us:

$$\begin{aligned} 3\frac{\ddot{a}}{a} &= -\frac{\kappa^2}{2}\langle\rho\rangle + \mathcal{Q}, \\ 3\left(\frac{\dot{a}}{a}\right)^2 &= \kappa^2\langle\rho\rangle - \frac{1}{2}\left\langle {}^{(3)}R\right\rangle - \frac{1}{2}\mathcal{Q}, \\ \mathcal{Q} &\equiv \frac{2}{3}\left(\left\langle\Theta^2\right\rangle - \langle\Theta\rangle^2\right) - 2\left\langle\sigma^2\right\rangle. \end{aligned} \tag{3.22}$$

Consider the first equation in (3.22) with the backreaction term expanded:

$$\begin{aligned} 3\frac{\ddot{a}}{a} &= -\frac{\kappa^2}{2}\langle\rho\rangle + \frac{2}{3}\left(\left\langle\Theta^2\right\rangle - \langle\Theta\rangle^2\right) - 2\left\langle\sigma^2\right\rangle, \\ \implies 3\frac{\ddot{a}}{a} &= -\frac{\kappa^2}{2}\langle\rho\rangle + \frac{2}{3}\left\langle\Theta^2\right\rangle - 6H^2 - 2\left\langle\sigma^2\right\rangle, \\ \implies q &= 2 - \frac{2}{9}\frac{\langle\Theta^2\rangle}{H^2} + \frac{1}{3}\left(\frac{\kappa^2}{2}\langle\rho\rangle + \frac{2}{3}\frac{\langle\sigma^2\rangle}{H^2}\right), \end{aligned} \tag{3.23}$$

where in going from the first to second step we rewrite the average of Θ as $3H$, and in going to the third step we divide both sides by $-3H^2$ to get the deceleration parameter on the left hand side. Compare this form of the averaged equation to the averaged equation obtained in the n-patch toy model (3.19) rearranged for convenience:

$$q = 2 - 2\frac{1}{H^2}\sum_i^n v_i H_i^2 + \frac{1}{H^2}\sum_i^n v_i H_i^2 q_i, \tag{3.24}$$

where the H^2 in the denominator is the averaged Hubble parameter, while the H_i are the non-averaged, local Hubble parameters within each region. H_i can be replaced by the volume expansion rate within each of the spherical perturbations as $H_i = \Theta_i/3$. Then the second term is the volume-weighted sum of Θ_i^2 (in some sense, an *averaging* in the toy model), which is the second term of the final form in equation (3.23). Now, the third term in equation (3.24) can be simplified by rewriting $H_i^2 q_i$ as $-\frac{\ddot{a}}{a}$. This, for an FRW universe, is precisely (3.21).

A similar argument can be made for the expression for the Hubble parameter; the local patches obey the second of equation (3.20), while the average obeys the second of (3.22). Expanding the latter gives us:

$$
\begin{aligned}
3\left(\frac{\dot{a}}{a}\right)^2 &= \kappa^2\langle\rho\rangle - \frac{1}{2}\left\langle {}^{(3)}R\right\rangle - \frac{1}{3}\left(\left\langle\Theta^2\right\rangle - \langle\Theta\rangle^2\right) + \left\langle\sigma^2\right\rangle, \\
\implies 3\left(\frac{\dot{a}}{a}\right)^2 &= \kappa^2\langle\rho\rangle - \frac{1}{2}\left\langle {}^{(3)}R\right\rangle + \left\langle\sigma^2\right\rangle - \frac{1}{3}\left\langle\Theta^2\right\rangle + \frac{1}{3}\langle\Theta\rangle^2.
\end{aligned}
\tag{3.25}
$$

In the toy model, this can be rewritten as:

$$
\begin{aligned}
3\left(\frac{\dot{a}}{a}\right)^2 &= \sum_i v_i\left(\kappa^2\rho - \frac{1}{2}{}^{(3)}R + \sigma^2\right) - \frac{1}{3}\left\langle\Theta^2\right\rangle + \frac{1}{3}\langle\Theta\rangle^2, \\
\implies 3\left(\frac{\dot{a}}{a}\right)^2 &= \frac{1}{3}\sum_i v_i\Theta_i^2 - \frac{1}{3}\left\langle\Theta^2\right\rangle + \frac{1}{3}\langle\Theta\rangle^2, \\
\implies \left(\frac{\dot{a}}{a}\right)^2 &= \frac{1}{9}\langle\Theta\rangle^2.
\end{aligned}
\tag{3.26}
$$

Squaring equation (3.18) gives us the same. With this equivalence, we have matched the toy model (3.19) to the averaged Buchert equations (3.22), thus confirming the origin of the backreaction term. Note that this term arises precisely because of the non-commutativity of time-evolution and spatial averaging. We can now proceed to characterize the evolution in each of the regions.

The spherical collapse model

The toy model above gives us the dynamics of the universe in terms of the dynamics within the individual regions. We must, hence provide a formalism for the evolution of these 'isolated regions'. The key formulae are summarized below, the notation borrowed from [SV04]. For rigorous justification and derivations, see the Appendix 6 of the thesis.

For the considerations of our toy model, we shall assume an EdS background, corresponding to $\Omega_b = 1$. All the trajectories are parameterized by a *development angle*, and the quantities of relevance to our numerical simulations are summarized here for completeness. The physical distance and time[7] are related as:

[7] The time coordinate t is the background EdS cosmic time that foliates our spacetime; the offset time T determines the 'orientation' of our foliation (see section 1.2) by fixing the state of the perturbation at each value of the cosmic time. All these considerations are subject to a vanishing vorticity that allows for such a foliation in the first place.

$$r\left(\phi\right)=\begin{cases}\frac{r_i}{2}\frac{1+\delta_{ci}}{\delta_{ci}}\left(1-\cos\phi\right) & \delta_{ci}>0,\\ \frac{r_i}{2}\frac{1+\delta_{ci}}{(-\delta_{ci})}(\cosh\tilde{\phi}-1) & \delta_{ci}<0.\end{cases}\tag{3.27}$$

$$t(\phi)+T=\begin{cases}\frac{1}{2H_b}\frac{1+\delta_{ci}}{(\delta_{ci})^{3/2}}\left(\phi-\sin\phi\right) & \delta_{ci}>0,\\ \frac{1}{2H_b}\frac{1+\delta_{ai}}{(-\delta_{ci})^{3/2}}(\sinh\tilde{\phi}-\tilde{\phi}) & \delta_{ci}<0,\end{cases}\tag{3.28}$$

The remaining quantities are given by:

$$H_{\delta^+}=\frac{\sin\phi(\phi-\sin\phi)}{B(1-\cos\phi)^2},\qquad H_{\delta^-}=\frac{\sinh\tilde{\phi}(\sinh\tilde{\phi}-\tilde{\phi})}{B(\cosh\tilde{\phi}-1)^2},$$
$$s_{\delta^+}\equiv\frac{a^3_{\delta^+}}{a^3_{\rm EdS}}=\frac{2(1-\cos\phi)^3}{9(\phi-\sin\phi-\frac{T}{B})^2},\qquad s_{\delta^-}\equiv\frac{a^3_{\delta^-}}{a^3_{\rm EdS}}=\frac{2(\cosh\tilde{\phi}-1)^3}{9(\sinh\tilde{\phi}-\tilde{\phi}-\frac{T}{B})^2},$$
$$q_{\delta^+}=\frac{1-\cos\phi}{\sin^2\phi},\qquad q_{\delta^-}=\frac{\cosh\tilde{\phi}-1}{\sinh^2\tilde{\phi}}.$$

Here, δ_{ci} is the initial density contrast of the perturbation relative to the *critical density*, not the average density as usually performed. δ^+ corresponds to an overdense region (which is also what the condition $\delta_{ci}>0$ is), while δ^- is an underdense region. The multiplication with factors of t is performed to make the relevent quantities dimensionless. Finally, notice the symmetry under trigonometric $\leftrightarrow$ hyperbolic functions that leads to the dynamics of over and under dense regions. The development angles are labelled differently to signify the difference in domain of values that they can take. The trajectory of an overdense region is that of a cycloid, and so ϕ takes values in $[0,2\pi]$; the underdense trajectories by virtue of being hyperbolic have $\tilde{\phi}$ range from $[0,\infty)$. The trajectory of an overdense region is bounded; the underdense region expands 'out to infinity'. The critical density profile has radial motion that obeys:

$$r(t)=\left\{\frac{3}{2}H_i\left(1+\delta_{ci}\right)^{1/2}t\right\}^{2/3},\quad \delta_{ci}=0.\tag{3.29}$$

The remaining quantities are given by:

$$H_{\rm EdS}t=\frac{2}{3},\quad s_{\delta^0}=1,\quad \left\langle{}^{(3)}R\right\rangle_{\delta^0}=0,\quad \delta^0=0.\tag{3.30}$$

Numerical analysis

There are three parameters that can be varied in the above model: the combination of densities (sign and magnitude), the volume fractions the regions occupy at some particular time, and the time of seeding of these volume fractions. This is characterized in detail in Appendix (6). The key conclusions and results are listed below.

A note on setting volume fractions as a free parameter: our spherical collapse model as in Appendix 6 gives us the physical radius of a spherical perturbation in term of the initial radius; the value of r_i itself is not predetermined. We do know that as the global EdS time goes to zero, we require all radii to go to zero, but this is accounted for by the offset time T. We are therefore at liberty to fix r_i for each region; this amounts to fixing the relative volumes of the regions at some global time of convenience.

Summary

The key effects of each of the variable parameters is summarized below:

1. The system accelerates if and only if there is an underdense region matched with an overdense region. Once this condition is met, the qualitative profile of the graph remains unchanged.

2. The overdense regions dictate how long the deceleration parameter remains negative, and in the cases of lower volume fractions, the time at which the minima is attained. Lesser the overdensity, more the time it takes to achieve $q_{\min}$.

3. The overdensities, irrespective of volume fraction, have no effect on the value of $q_{\min}$ if the other region is empty. Greater the volume fraction imparted to the overdense region, greater the maximum acceleration observed.

4. As we move towards a less underdense region, the effect of the overdense region becomes more pronounced; a greater acceleration is observed for a more overdense region.

5. Irrespective of the volume fractions imparted, the value of the underdensity has a greater effect on the acceleration than an overdensity; lesser the underdensity, greater the acceleration.

6. Volume fractions have by far the greatest effect on the quantitative profile of the graph; a higher acceleration is seen if a smaller volume fraction is given to the underdense regions.

7. Volume fractions also determine whether or not the value of $q_{\min}$ is dictated by the virialization of overdense regions; a greater volume fraction imparted to the overdense regions pulls the minima to a time before virialization.

To summarize the summary, if we want a greater, prolonged acceleration, assign a smaller overdensity (for having an acceleration for longer) and a lesser underdensity, while imparting a smaller volume fraction to the underdensity. If we do not require the acceleration to be prolonged, then retain all the above parameters while making the overdense region more overdense.

Heuristic justification:

Observing acceleration due to inhomogeneity can intuitively be explained by the increase in volume fraction of underdense regions (that expand forever albeit at a decelerating rate) relative to overdense regions that either collapse to a singularity or virialize to form structures (thus effectively halting their time). In light of this hand-wavy explanation, it is interesting to ask how the above observations may be interpreted to affect the volume fractions.

Clearly, the volume fraction of an underdense region can contribute significantly only if the other region begins shrinking and eventually stops growing in time. Therefore, two underdense regions can never show an acceleration. In the presence of two overdense regions, there technically *can* be a period of acceleration if one overdense region is significantly more overdense than the other, if the more overdense region begins to collapse while the other region still expands. However, the deceleration parameter diverges quickly to a positive value before a *brief* period of acceleration, which quickly dies out to a positive value of q again. A lower overdensity means that it takes longer for the region to virialize after turnaround, so the the volume of the overdense region decreases for a longer period of time. So, the effect it has on increasing the volume fraction of the underdense region is more prolonged. This explains observations 1 and 2.

Now, the volume fraction of say, an empty and overdense region go as:

$$v_o = \frac{\delta_o (r_i)_o^3 (t^{2/3} - t^{4/3})}{\delta_0 (r_i)_o^3 (t^{2/3} - t^{4/3}) + (r_i)_e^3 t^3}, \quad v_e = \frac{(r_i)_e^3 t^3}{\delta_o (r_i)_o^3 (t^{2/3} - t^{4/3}) + (r_i)_e^3 t^3}, \tag{3.31}$$

where the scale factor for the empty region goes as t^3, and to the two leading terms for the overdense region goes as $\delta_o(t^{2/3} - t^{4/3})$. For an underdense region, the analogous approximation would be $\delta_u(t^{2/3} + t^{4/3})$. Here, since t^3 grows much faster than the scale factor, the value of the overdensity doesn't at all affect the dynamics of volume fractions. However, the perceived growth of an underdense region increases if the contribution in the denominator from δ_o is greater. This is why in general for an underdense region, the maximum acceleration increases for a more overdense partner. A similar argument can be made for the choice of volume fractions. If the volume fraction of the overdense region is greater, then the denominator can be dominated by the overdense term, which is why any incremental increase in the volume fraction of an underdense or empty region appears greater. Conversely, if a low volume fraction is allotted to the overdense region, the denominator is dominated by the underdense or empty term, and so the volume fraction does not increase as much for the same increment in the numerator. These rough arguments could explain observations 3 to 5. Finally, the reason volume fractions have the greatest effect is because they appear as a r_i^3, as opposed to the densities, that appear as a linear δ. Assigning a smaller initial radius to the overdense region has a smaller effect on the denominator during collapse; it is the contrast of the relative magnitudes of the initial radii of the two regions that makes volume fraction of the underdense region rise rapidly post-turnaround. This explains observations 6 and 7.

3.2.2 Gaussian-random distribution

The 2-region model is quite successful in qualitatively accounting for an accelerated expansion, but is not physically realistic in its distribution of initial distribution of density perturbations. Ideally, we would like to put the backreaction model to test on the perturbation profile of the Cosmic Microwave Background (CMB), whose power spectrum we know to very high precision. This was done in [Räs08a], where the authors attempted to formulate a multi-region extension of the 2-region model, while drawing the distribution of densities from a Gaussian random distribution.

The key arguments and results are summarized here. The universe is still considered a union

of isolated, spherically symmetric regions with linear density contrast δ. The initial density perturbation profile is assumed to have a Gaussian spectrum with homogeneity scale R. In order to perform constant time averages as before, we require a notion of volume fractions. This is given by:

$$v_\delta(t) = \frac{\int_{t,\delta} \epsilon}{\int_t \epsilon}, \tag{3.32}$$

where the numerator is the volume of the region of density contrast δ. Assuming we start with perfect homogeneity and isotropy, we may assume that each region at some time represents a particular stage of collapse. This is tantamount to making a 1-1 correspondence of the linear density contrast δ with the average expansion rate of the region. The net Hubble parameter is then, again, the sum of volume weighted Hubble parameters of the individual regions, now expressed as an integral:

$$H(t) = \int_{-1}^{\infty} v_\delta(t) H_\delta(t) d\delta = \frac{\int_{-1}^{\infty} s_\delta f(\delta, t) H_\delta(t) d\delta}{\int_{-1}^{\infty} s_\delta f(\delta, t) d\delta}. \tag{3.33}$$

Here, the volume fraction is split in two parts: s_δ being the ration of the cubes of the scale factors within the region and the EdS background, and $f(\delta, t)$ being the initial volume fractions at the time of seeding. For Gaussian random perturbations, we have an analytic expression for the number densities ($n(\nu, R)$; $\nu \equiv \delta/\sigma_0(t, R)$) of peaks of a particular value of density contrast. This quantity can be used as the number density of isolated regions having that linear density contrast. This then can be used to quantify the mass enclosed within all overdensities of that density contrast, which then under the assumption of a smooth universe initially, can be converted to a volume fraction.

We have now related the *initial* volume fractions to the number density of peaks of the initial Gaussian random profile. In order to relate this to later times, they make use of a *transfer function* that relates the initial power spectrum of density perturbations to the one observed at present. A detailed quantitative analysis is presented in the paper; the result when finally implemented was a universe that *neither accelerated, nor decelerated*. The deceleration parameter fell monotonically to zero, despite the dimensionless Hubble parameter increasing at all times. There were a number of reasons cited for this apparent failure to show an accelerated expansion, one being that the overdensities were not prominent

enough to initially bring the Hubble parameter down before having it increase. Since the deceleration parameter is a measure of the rate of change of H, an increase in the Hubble after an initial decrease results in a contrast that makes q negative. This, and other factors are further elaborated on in the next section.

3.3 Drawbacks

The task of working within the formalism of General Relativity without any local symmetries is a formidable one; indeed, in the presence of inhomogeneity and anisotropy, we no longer have a metric that is valid locally at *every* point. This is what motivated our approaching the EFEs through a spacetime threaded by fundamental worldlines, as opposed to a foliation that reflected symmetries that could be imposed on a metric.

There are two classes of drawbacks that need to be addressed: those on the formalism itself, and the ones on the toy models. Perhaps the most glaring issue with the averaging formalism is the fact that all averages and calculations (scale factors, densities etc) are performed on a surface of *global simultaneity*, and not on the hypersurface that is *causally connected*. This means that all predictions made cannot be tested against observable data. There really is only one way to rectify this, and that is to define a *light-cone average* that takes into consideration the actual path of a ray of light. This task is daunting, and perhaps impossible to implement without a statistical treatment of the distribution of inhomogeneities. We will be required to introduce an embedding of the regions in a background, and account for a differential evolution in the regions as a result of the finitude of c. All is not lost, however. One way to motivate our considering this formalism at all is to think of an acceleration in a hypersurface of global simultaneity as a sure-shot check of whether any acceleration can be *perceived*. If the volume (of global simultaneity) an *every* instant of time *truly* accelerates, then there must be a perceived acceleration in the path of light as well. However, to check the extent to which a backreaction term can account for an acceleration, we must introduce a light cone average to make any comparisons.

The second drawback to the formalism (also mentioned earlier) is the requirement of a vanishing vorticity on every observer. Vorticity is perhaps the greatest contributing factor to stabilizing the collapse of overdense regions via virialization; thermalization and radiation being two prominent others. There is a treatment that can be imparted to small vorticities, see [Mag12] for a description of the same. However, this too is just band-aid over cancer; a

smooth foliation is simply impossible in the presence of vorticity.

Toy models, by virtue of being idealizations, are rife with scope for improvement. Their significant insights notwithstanding, they must be brought closer to reality for the formalism of inhomogeneities to hold water. The two-region model while showing remarkable likeness to the results from the ΛCDM model, does not account for the way the regions are embedded in a background, and as a result makes no comments on the dynamics the background. The spherical collapse model tacitly assumes the background to have an EdS profile, and the toy model makes no reference to a background expansion at all. Further, an explicit embedding will enforce a measure of separation between the regions, and so care must be taken to model the overlap of the two regions and the transfer of mass. This in fact brings to light another issue, which is that the regions are taken to be non-interacting. In the physical universe, overdense regions become more dense with time by accreting matter from a neighbouring underdense region. This could, potentially, increase the acceleration perceived in the toy model, and so in that sense, a non-interacting formalism acts as a lower bound to the acceleration. Other idealizations include setting the shear to zero (which is addressed in [BC08]) and considering a pressure-free dust that does away with thermalization. Note that the presence of shear has a diminishing effect on the magnitude of the backreaction, and so this particular idealization represents a best-case scenario.

The model that inputs Gaussian random perturbations from the CMB, while starting out with a more realistic density profile, still considers its individual regions as isolated and makes no mention of an embedding. Further, as mentioned by the authors themselves, a major contributing factor to acceleration could be the formation of structure (modelled as groups of overdensities and underdensities within a particular region; the universe being a union of such regions).

Structure formation cannot be modelled by grouping regions together and recursively applying the equations (3.17 - 3.19). Consider n isolated regions, each of which are a collection of different regions themselves. Since equations (3.17 - 3.19) are constructed for a general number of patches, we may assume that they apply both within each of the n regions, and to the n regions as a whole as well. So, we have:

$$a_{(n)} = \left(\sum_i^n a_i^3 \right)^{1/3}, \quad H_{(n)} = \sum_i^n v_i H_i, \quad q_{(n)} = 2 + \frac{1}{H_{(n)}^2} \sum_i^n v_i H_i^2 (q_i - 2), \tag{3.34}$$

and

$$a_{(i)} = \left(\sum_{i'}^j a_{i'}^3 \right)^{1/3}, \quad H_{(i)} = \sum_{i'}^j \lambda_{i'} H_{i'}, \quad q_{(i)} = 2 + \frac{1}{H_{(i)}^2} \sum_{i'}^j \lambda_{i'} H_{i'}^2 (q_{i'} - 2), \tag{3.35}$$

where the volume fractions v_i are weighted against the volume of the entire system, but the volume fractions $\lambda_{i'}$ are weighted against the volume of the respective smaller regions that they are a part of. We thus have the trivial relations: $v_i = v_i \sum \lambda_{i'}$ and $v_i \lambda_{i'} = v_{i'}$. The above equations can be applied recursively for as many groupings we wish to perform; the substitution is performed once only for demonstration. The Hubble parameter being volume-weighted means that the form doesn't change upon recursion. The same goes for scale factor. The deceleration parameter is now calculated as:

$$\begin{aligned}
q_{(n)} &= 2 + \frac{1}{H_{(n)}^2} \sum_i^n \left[v_i H_i^2 \left(2 + \frac{1}{H_{(i)}^2} \sum_{i'}^j \lambda_{i'} H_{i'}^2 (q_{i'} - 2) - 2 \right) \right] \\
&= 2 + \frac{1}{H_{(n)}^2} \sum_i^n \left[v_i H_i^2 \left(\frac{1}{H_{(i)}^2} \sum_{i'}^j \lambda_{i'} H_{i'}^2 (q_{i'} - 2) \right) \right] \\
&= 2 + \frac{1}{H_{(n)}^2} \sum_i^n v_i \sum_{i'}^j \lambda_{i'} H_{i'}^2 (q_{i'} - 2) \\
&= 2 + \frac{1}{H_{(n)}^2} \sum_{i'}^j \sum_i^n v_i \lambda_{i'} H_{i'}^2 (q_{i'} - 2) \\
&= 2 + \frac{1}{H^2} \sum_{i'} v_{i'} H_{i'}^2 (q_{i'} - 2).
\end{aligned} \tag{3.36}$$

Since the functional form of the deceleration parameter is the same irrespective of grouping, the interpretation of structure formation within regions cannot be imparted to the n-region model. The qualitative results obtained before can therefore be extended to any possible grouping of the regions. This is an artefact of the fact that the deceleration parameter of the individual regions enter the equation linearly when calculating the net deceleration

parameter, which in turn is because the regions are isolated from each other (that is, they do not see each other). This tells us that the only way to model structure formation is by introducing an interaction between regions.

The afore considerations are what motivate the following infinitesimal improvement to the toy models. The next chapter documents our attempt to introduce an interaction between (and hence an embedding of) regions to model structure formation through a mass-transfer across regions.

Chapter 4

Improved Model

4.1 Inducing interactions

In section 3.3, one of the drawbacks mentioned was the lack of explicit embedding in a background, and the fact that the regions were taken to be isolated. We also showed how 'grouping' isolated regions cannot be used to recursively impart an interpretation of structure formation. A group of regions can be thought of forming a 'structure' if they interact with each other gravitationally, but not as strongly with another group of similarly interacting regions. In order to define such a system, we must define a notion of *interaction* and *proximity*.

The method adopted here is to consider two regions as interacting if they are open relative to each other, i.e., they share a common boundary and can thus exchange mass. This is implemented in the following way: we initialize our universe with two regions, say one overdense and the other underdense (relative to an EdS background). These two spherical perturbations are initially in contact with each other tangentially. During their *initial* evolution over some discretized time step, they both expand slightly as they are dragged along with the background flow. This results in the two regions sharing a small volume of overlap. Since the overdense region has an expansion rate that is *slightly* smaller than the underdense region, the mass in the underdense region corresponding to the overlapping volume is considered completely transferred to the overdense region, distributed evenly in its volume at the updated time step. The overdense region retains any mass it had in the volume of overlap. The two regions then separate by the same amount that they overlap, thus making them tangential again. We then rinse and repeat until the overdense region

virializes, at which point it stops accreting mass. This is depicted visually below, where the smaller region is overdense while the larger one, underdense.

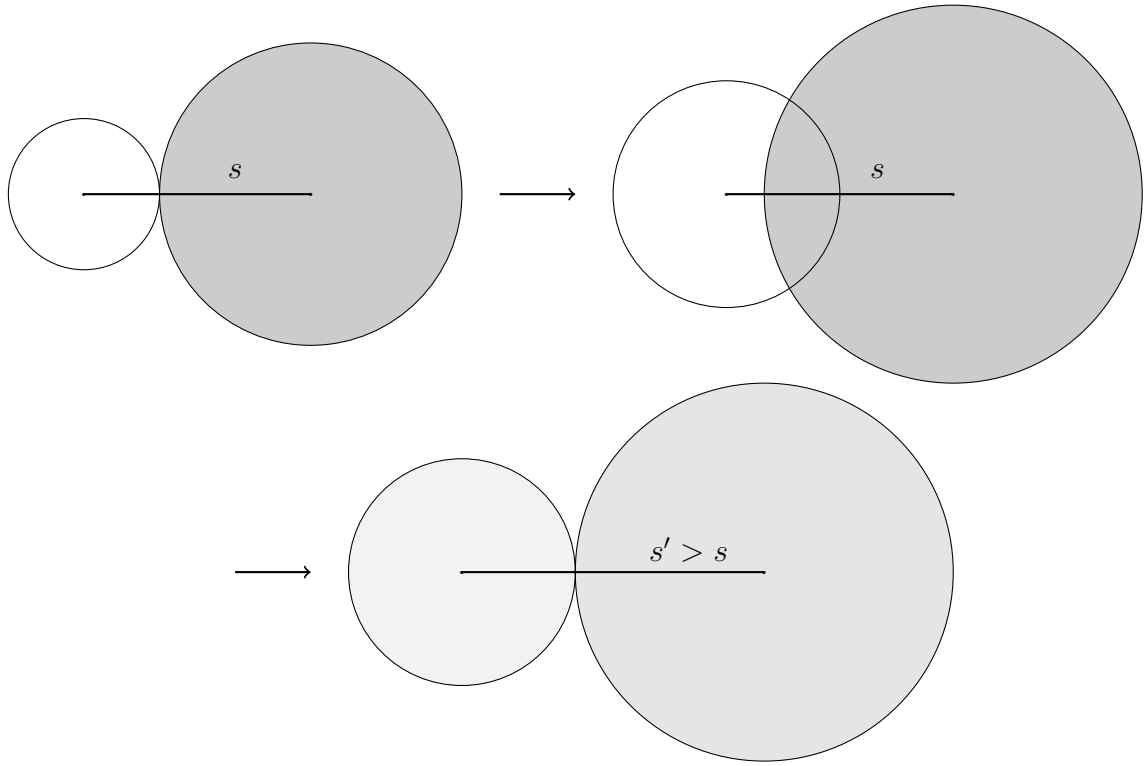

Okay! There is a lot to be justified and accounted for here. Firstly, despite the existence of a background flow, we do not (at least as a first approximation) account for the separation of the centres of the regions due to this flow. The two centres should ideally move apart slightly due to an EdS expansion in the time step considered. We neglect this because it would suggest that despite the existence of non-linear density perturbations at late-time, the universe on average continues to behave like an EdS one, which is exactly what we hoped to disprove. In shifting the centres by exactly the extent of overlap, we induce a background expansion by an amount that is dictated by the evolution of our regions *alone*.

Secondly, by making the two regions tangential at each time step, we are further insisting that our discretized timescale of evolution is large enough for the transferred mass to equilibrate uniformly within the overdense region, and for the underdense region to recover its loss by redistributing its remaining mass and attenuate its distortion to become spherical again.

Thirdly, the assumption of virialized structures halting accretion is not strictly true; overdense structures that have stabilized *do* accrete mass from neighbouring underdensities, but

at significantly greater timescales than when they haven't virialized. We shall therefore *assume* that our physics is relevant only up to the timescale of virialization, at which point we only evolve our universe for a small interval of time after.

Fourthly, the mass is always assumed to transfer from an underdense to an overdense region. The rationale here is that the underdense region has a greater outward velocity than the overdense region. A similar argument is to be made when we couple two underdense regions close to each other: the more underdense region will transfer mass to the less underdense region.

We must, finally, address the thorny issue of when virial equilibrium is achieved in the overdense region. Recall from Appendix 6 that this was fixed at half the radius of turnaround by finding the point at which the kinetic energy is equal to half the potential energy. The issue here is that since our system is open, we no longer conserve energy. The condition for virial equilibrium is hence ill-defined, apriori. There are two ways to deal with this, which are heuristically fleshed out below. In our implementation, we adopt the first approach, with the aim of studying the second later.

The first way to force a virialization is to simply *insist* that our overdensity stabilizes at a development angle of $3\pi/2$. This condition is borrowed blindly from the case where the energy was conserved with absolutely no justification, really. The second way is to at every point after turnaround, check if the radius for the particular value of density contrast at that instant happens to be half the theoretical maximum it should have been, had it started out with that value of density contrast. This latter approach is based on the fact that the coefficient of our trajectories are determined completely by the value of the initial density contrast and background Hubble parameter.

There is a small point to be made on the way the model is being implemented. Recall that the spherical collapse model is *defined* for systems with conserved mass (and hence energy). The *correct* method would be to obtain a corresponding differential equation for a variable-mass gravitational system, and implement it as an alternative to the spherical collapse model. There have been numerous attempts in that direction, an interesting one is explored in [CL90]. What we are doing here is to employ the more expedient approach of infinitesimally redefining our initial conditions on the spherical collapse model at each time step to correspond to the present radius, present Hubble parameter value, and the updated

density contrast with the gained (lost) mass.

4.2 Spherical Collapse revisited

In order to implement a modified spherical collapse model, we begin by altering the constant-mass algorithm to account for updated initial conditions. Recall that the entire trajectory was obtained from the initial density contrast δ_i, initial background Hubble expansion $H_b(t_i)$, and the initial radius r_i. The density contrast, however, changes with time. This is because while the mass within the boundary of (say) the overdense region remains the same, the region itself expands more slowly than the background EdS universe. As a result, the density inside does not dilute as fast as that outside. Its contrast with respect to the background hence increases. When measured relative to the background, an overdense region becomes more overdense, while the underdense more underdense.

We may, therefore, attempt to implement the same spherical collapse by at every discretized time step, updating our density contrast to the new one at that instant, while simultaneously updating the initial radius and background Hubble parameter as well. There is one issue we are overlooking here: that at late-times in the evolution of the region, the velocity of the perturbation will vary significantly from that of the background Hubble expansion. This must be accounted for, and the trajectories appropriately modified. Put differently, our cycloid trajecotry is determined completely by the initial radius (r_i), the initial velocity of our perturbation (which we assumed to equal the background Hubble rate H_i), and the density contrast. An appreciable peculiar velocity in the expansion of our perturbation can be accounted for in an overdense region, as follows.

Our objective is to go from a solution of the form

$$r = A_i(1 - \cos\theta), \quad t + T = B_i(\theta - \sin\theta); \quad A_i^3 = GMB_i^2, \tag{4.1}$$

to one of the form:

$$r_{t+\delta t} = A_t(1 - \cos\theta), \quad t + \delta t + T = B_t(\theta - \sin\theta); \quad A_t^3 = GMB_t^2. \tag{4.2}$$

This requires our determining the functional form of our updated coefficients. The kinetic

energy of the perturbation is no longer $\dot{r}_i^2 = H_b(t_i)^2 r_i^2$, but is $K_t = \frac{1}{2}\dot{r}_t^2 = \frac{1}{2}H_t^2 r_t^2$ at some time t, where $H_t = \frac{\dot{r}_t}{r_t}$ is the Hubble expansion of the region. The potential energy is then:

$$U_t = -\frac{GM}{r_t} = -\frac{G}{r_t}\left(\rho\frac{4\pi}{3}r_t^3\right)\left(\frac{\rho_b}{\rho_b}\right)\left(\frac{H_b^2}{H_b^2}\right),$$

where ρ_b and H_b are taken at time t. This can be rearranged to give:

$$U_t = -\frac{1}{2}H_b^2\Omega_b(t)r_t^2(1+\delta_t) = -\frac{H_b^2}{H_t^2}K_t\Omega_b(t)(1+\delta_t). \tag{4.3}$$

Here, Ω_b is the dimensionless density parameter of the background relative to an EdS universe; δ the density contrast of the perturbation with respect to the background. For an EdS background, $\Omega_b = 1$. The total energy is then given by:

$$E = K_t\Omega_b(t)\left[\Omega_b^{-1}(t) - \frac{H_b^2}{H_t^2}(1+\delta_t)\right], \tag{4.4}$$

and the condition for collapse ($E < 0$) in an EdS background is $\delta_t > \frac{H_t^2}{H_b^2} - 1$. The updated coefficients at every instant are obtained by comparing the total energy to the energy at turnaround for that particular density contrast, where the kinetic term goes to zero. At turnaround,

$$E = -\frac{GM}{r_m} = -\frac{r_t}{r_m}\frac{GM}{r_t} = -\frac{r_t}{r_m}\frac{H_b^2}{H_t^2}K_t\Omega_b(t)(1+\delta_t). \tag{4.5}$$

Equating this to the total energy gives us a ratio between the updated initial radius r_t and the maximum radius $r_m = 2A_t$, which can then be used to find the coefficient A_t (and hence also B_t:

$$A_t = \frac{r_t}{2}\frac{(1+\delta_t)}{\left(1+\delta_t - \frac{H_t^2}{H_b^2}\right)}, \quad B_t = \frac{1}{2H_b(t)}\frac{(1+\delta_t)}{\left(1+\delta_t - \frac{H_t^2}{H_b^2}\right)^{3/2}}. \tag{4.6}$$

There will be a modification to the calculation of successive density contrasts as well. We have $\rho_t = \frac{3M}{4\pi A_t^3(1-\cos\theta)^3}$ and $\rho_b = \frac{1}{6\pi G t^2} = \frac{1}{6\pi G(B_t(\theta-\sin\theta)-T)^2}$, where we recognise that the EdS background time must account for the offset time T that our overdense region measures. Then:

$$\frac{\rho_t}{\rho_b} - 1 = \delta_t = \frac{9}{2}\frac{(\theta - \sin\theta - T/B_t)^2}{(1-\cos\theta)^3} - 1, \tag{4.7}$$

where we have made use of $A_t^3 = GMB_t^2$. The underdense regions have:

$$A_t = \frac{r_t}{2}\frac{(1+\delta_t)}{\left(\frac{H_t^2}{H_b^2} - (1+\delta_t)\right)}, \quad B_t = \frac{1}{2H_b(t)}\frac{(1+\delta_t)}{\left(\frac{H_t^2}{H_b^2} - (1+\delta_t)\right)^{3/2}}, \tag{4.8}$$

and:

$$r_{t+\delta t} = A_t(\cosh\theta - 1), \quad t + \delta t + T = B_t(\sinh\theta - \theta); \tag{4.9}$$

$$\delta_t = \frac{9}{2}\frac{(\sinh\theta - \theta - T/B_t)^2}{(\cosh\theta - 1)^3} - 1. \tag{4.10}$$

It can easily be checked that both formulations when evolved numerically result in identical physics. Now that we have this implementation of the spherical collapse model, all that remains for us to do is quantify the amount of mass that gets transferred from the underdense to overdense region, and add that additional mass to δ_t at each time step!

The first calculation we perform is to calculate the volume of overlap at each time step. When initialized, the centres of the two spherical regions are separated by a distance of $s^t = r_1^t + r_2^t$, where we shall henceforth always subscript the overdense region with 1 and the underdense one as 2. At $t + \delta t$, the radii evolve according to the equations above to $r_1^{t+\delta t}$ and $r_2^{t+\delta t}$, while the centres remain at the same separation s^t. To find the volume of overlap, it is useful to define a few variables as in the diagram below:

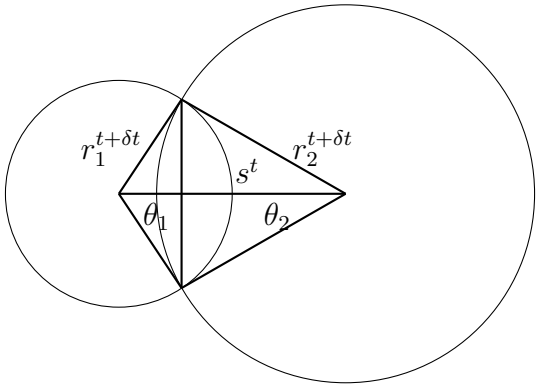

The angles θ_1 and θ_2 are calculated from:

$$\begin{aligned} r_1^{t+\delta t}\sin\theta_1 &= r_2^{t+\delta t}\sin\theta_2 \\ r_1^{t+\delta t}\cos\theta_1 + r_2^{t+\delta t}\cos\theta_2 &= s^t; \end{aligned} \tag{4.11}$$

the solution to which is:

$$\begin{aligned} \theta_1 &= \cos^{-1}\left(\frac{(r_1^{t+\delta t})^2 - (r_2^{t+\delta t})^2 + (s^t)^2}{2s^t r_1^{t+\delta t}}\right) \\ \theta_2 &= \sin^{-1}\left(\frac{r_1^{t+\delta t}}{r_2^{t+\delta t}}\sin\theta_1\right). \end{aligned} \tag{4.12}$$

The volume of overlap is obtained by dividing it into two regions as defined by a vertical plane that is depicted as the vertical line above. Each of the two regions is obtained by subtracting the volume of the cone from the corresponding solid sector of the sphere, given that we have the angles θ_i. The volume of overlap is then given by:

$$V_{\rm ov}^{t+\delta t} = \sum_i \frac{\pi(r_i^{t+\delta t})^3}{3}(2 - 2\cos\theta_i - \sin^2\theta_i\cos\theta_i). \tag{4.13}$$

The mass from the underdense region enclosed within the volume of overlap is given by $\delta m = V_{\rm ov}\rho_2^{t+\delta t}$, and so the density in the overdense region changes by:

$$\rho_1(t+\delta t) = \rho_1^{t+\delta t} + \frac{V_{\rm ov}\rho_2^{t+\delta t}}{V_1^{t+\delta t}}. \tag{4.14}$$

We now substitute: $\rho_i^{t+\delta t} = \rho_b(1+\delta_i^{t+\delta t})$ to get:

$$\begin{aligned} \delta_1(t+\delta t) &= \delta_1^{t+\delta t} + (1+\delta_2^{t+\delta t})\frac{V_{\rm ov}}{V_1^{t+\delta t}} \\ \delta_2(t+\delta t) &= \delta_2^{t+\delta t} - (1+\delta_2^{t+\delta t})\frac{V_{\rm ov}}{V_2^{t+\delta t}}. \end{aligned} \tag{4.15}$$

These density contrasts will now be used to update our coefficients, thus effecting a variable mass system of equations that conserve mass across both regions, but not individually.

4.3 Preliminary Results

Before looking at what our simulations actually yield, we can place our bets on what we may expect. When pairing two overdense regions, we transfer mass from the less dense region to the more overdense one. As long as they both remain 'overdense' relative to the background, the results should not differ qualitatively from the isolated 2-region model. If the less dense one were to lose mass to the extent of becoming underdense over time, then we could potentially see an accelerated expansion for a brief period of time, provided the other overdense region hasn't virialized already. This situation is unlikely, however, as will be seen shortly. The collapse and virialization of the accreting region will happen much before a change in curvature could manifest in the other region.

When pairing an overdense region with an underdense one, the overdense region gets more dense, while the underdense region gets emptier with time. Since the acceleration is as a result of the collapse of the overdense region and the resultant interplay between volume fractions, we should expect our system to begin accelerating earlier, but also expect the acceleration to die out quickly owing to a faster virialization.

Finally, we could pair two underdense regions together and ask if the less underdense one could accrete enough mass to flip its curvature around and begin to collapse. This, unlike the overdense duo, should happen if the system is evolved long enough.

When evolving the system numerically, a very small discretized time interval would not result in an appreciable mass being transferred across regions, and the outcome wouldn't differ much from the isolated model. However, selecting too large a time-step could also lead to numerical difficulties. There is hence a Goldilocks's zone that gives us a perceivable change, while still being numerically tractable. Notice that since we haven't fixed explicit units for our time, we have a little freedom in the choice of our time interval of mass-transfer.

4.3.1 $\delta_1 > 0$, $\delta_2 < 0$

There are two effects that are potentially at play here: the time-step (as mentioned before), and the density contrast of the underdense region. If the underdense region has $-1 \lesssim \delta < 0$, it will grow much faster leading to a greater volume of overlap, but hold too dilute a mass concentration to transfer a substantial amount of it, independent of the size of the time step. This is demonstrated below, where we hold the overdense region constant at a contrast of

0.5, while pairing it with an underdensity of -0.4 and -0.9.

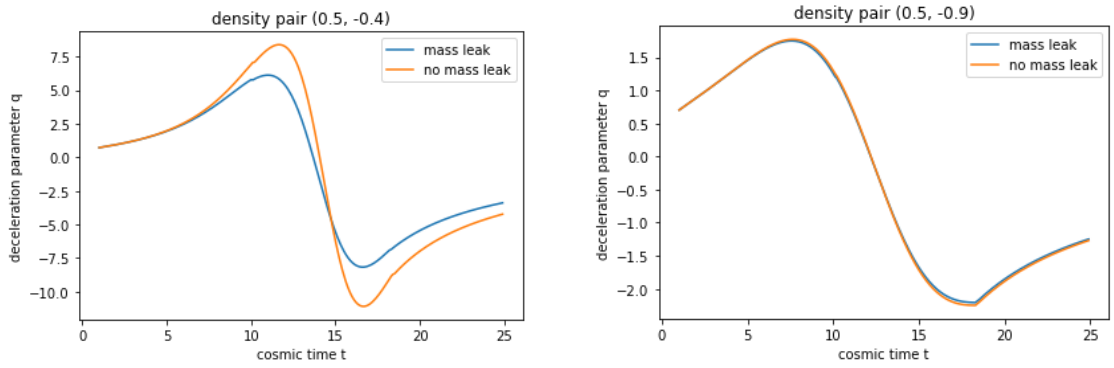

Figure 4.1: Graph of the deceleration parameter for two possible underdensities against the same overdensity; compared with the isolated region model. The volume fractions correspond to (0.3, 0.7) at the time of turnaround of the overdense region. The time step is taken identically for all three simulations.

There is negligible difference between the isolated region model and the open system model when the underdensity is close to being empty. There is also much to be noted from the first graph above: the existence of an interaction pulls q to a negative value more quickly, but q begins to approach 0 asymptotically much sooner as well. This is because the overdense region virializes (reaches a development angle of $3\pi/2$) faster. The radius of the overdense region, dimensionless Hubble parameter and densitiy contrasts are compared for the isolated and interacting model below, for the pair (0.5, -0.4):

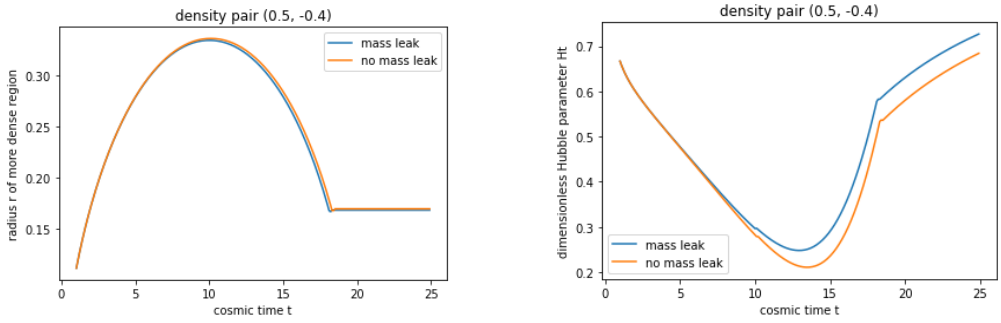

Figure 4.2: Graph of the radius and dimensionless Hubble parameter for (0.5, -0.4); compared with the isolated region model with the same pair. The volume fractions correspond to (0.3, 0.7) at the time of turnaround of the overdense region.

The density contrast increases (falls) more steeply for the overdense (underdense) region, as seen:

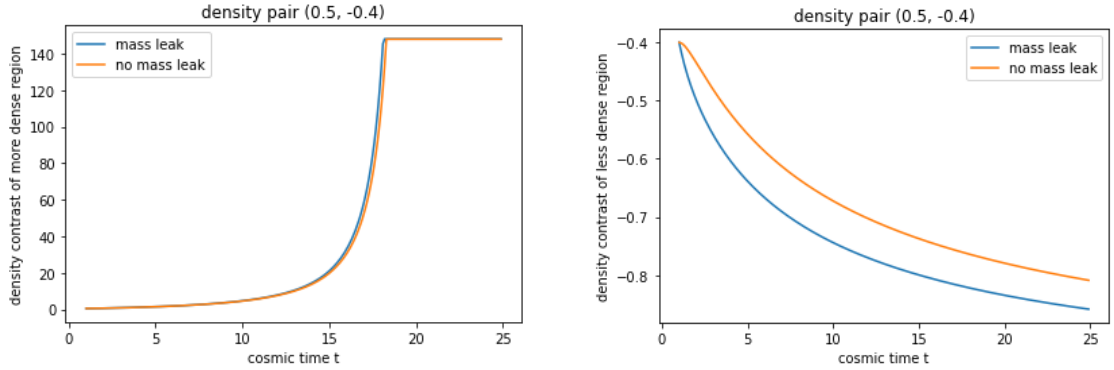

Figure 4.3: Graph of the density contrast of over and under dense regions; compared with the isolated region model. The volume fractions correspond to (0.3, 0.7) at the time of turnaround of the overdense region.

The density contrast of the overdense region is seen to plateau upon virialization. This is strictly not true; as the background keeps expanding, the density contrast should ideally increase slowly as well. This was not implemented out of numerical expedience; the precise approach, however, would lead to the same results in the time domain of interest (which in our case, is the time up to virialization). We now keep the underdensity fixed at -0.4 and vary the overdensity:

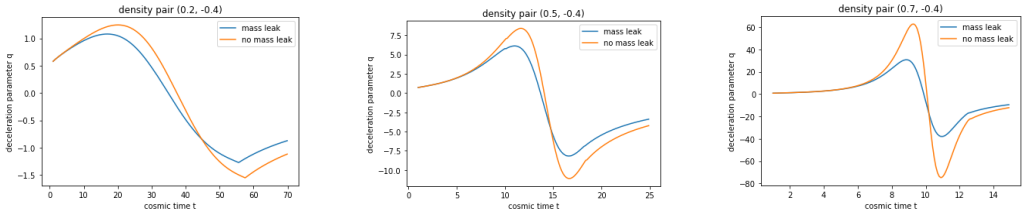

Figure 4.4: Graph of the deceleration parameter for two possible underdensities against the same overdensity; compared with the isolated region model. The volume fractions correspond to (0.3, 0.7) at the time of turnaround of the overdense region. The time step is taken identically for all three simulations.

The above plot makes corroborates our theory of the effect of an increasing overdensity; the faster our region collapses, the more it diminishes both the deceleration *and* acceleration.

4.3.2 $\delta_1, \delta_2 < 0$

This is where things could get interesting! Recall that two underdense regions *never* accelerate in the isolated region model. The question is, can we accrete enough mass and flip our curvature fast enough to result in an accelerated expansion? Well, no[1].

Two isolated underdensities have a deceleration parameter that asymptotically approaches zero from a positive value. In order to break away from this behaviour, we need a rapid change in the smaller underdensity to reverse curvature and achieve a collapse. There are two competing effects at play: the denser underdensity has a contrast that reduces in time owing to its own expansion relative to the background, and an increase in contrast from the mass it accretes from its partner. Therefore, the increase from the mass accreted needs to outweigh reduction from its own expansion. This cannot happen unless we assign a greater volume fraction to the emptier region. However, recall from the isolated region model, that an overdensity must have a greater volume fraction to significantly contribute to the denominator of volume-weighted quantities. This, it appears, means that two underdensities with a mass transfer still show an asymptotic fall of q to zero from a positive value, but just faster. This is shown in the graph below.

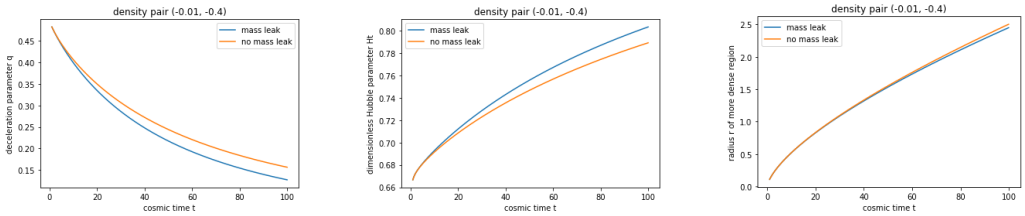

Figure 4.5: Graph of two underdense regions; compared with the isolated region model. The initial radii are around (0.11, 0.04). The time step is taken identically for all simulations.

The above figures assign a greater volume fraction to the less dense region. The densities contrasts evolve as below in Fig. 4.8. Notice that while the contrast of the more dense region initially increases, it drops again.

The same quantities are plotted by assigning a greater volume fraction to the emptier region, below. This time, we see that the more dense region attains a positive density contrast, but

[1]Sigh! To quote the great *philosopher* Mick Jagger, *"You can't always get what you want,"* and no matter how hard you try, you sometimes can't get what you need, either.

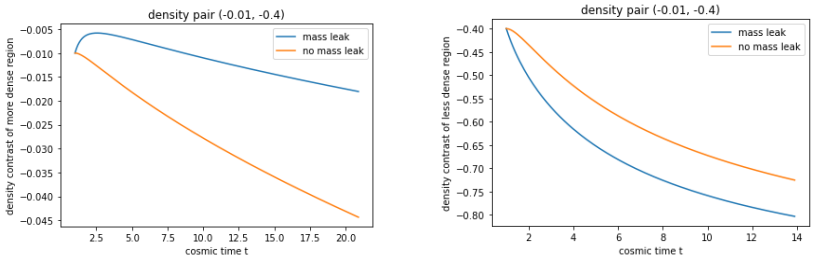

Figure 4.6: Graph of density contrasts of two underdense regions; The initial radii are around (0.11, 0.04). The time step is taken identically for all three simulations.

doesn't have any effect on the dynamics of the net deceleration parameter.

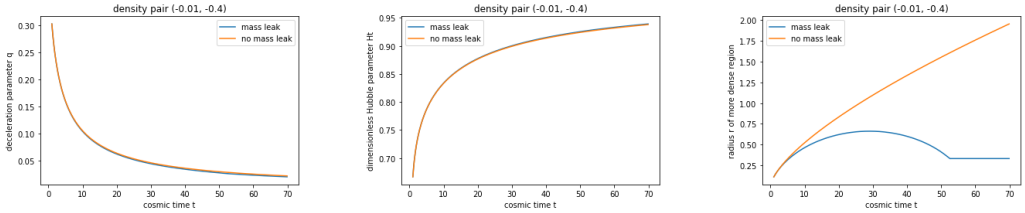

Figure 4.7: Graph of two underdense regions; compared with the isolated region model. The initial radii are around (0.11, 0.4). The time step is taken identically for all simulations.

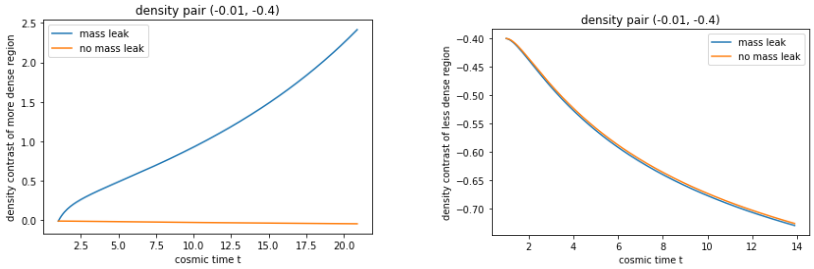

Figure 4.8: Graph of density contrasts of two underdense regions; The initial radii are around (0.11, 0.4). The time step is taken identically for all three simulations.

Chapter 5

Discussion and Future Work

Alright! Let us first summarize all that has been achieved so far. We started by recognising that the formation of structure in the non-linear regime from linear density perturbations should not be well-represented by the averaged equations, i.e., the FLRW paradigm, owing to the non-linear nature of the Einstein Field Equations. In order to study the effect of inhomogeneity on the average expansion of the universe, we shifted our approach to the formalism from a foliation to a threading on which we defined local surfaces that had to be patched together. We then met the Buchert averaging procedure and studied a few toy models that attempted to qualify the extent to which the resultant backreaction term could effect an accelerated expansion in the universe.

Building on extant literature, we introduced an explicit embedding of regions and defined a notion of proximity, both of which were absent in the toy models. We saw that the transfer of mass across regions under some constraints could result in a quicker and more pronounced acceleration in the spatial domain of interest, and even flip the sign of the curvature under certain conditions, albeit not to the extent that we would have liked.

There is much work to be done at this juncture! Now that our regions are no longer isolated, we can impart a notion of structure formation by grouping a finite number of regions together that share mass, and study the net acceleration perceived in a system of relatively isolated regions that have this nested structure. Recall (from section 3.3) that such an interpretation could not be imparted to isolated regions alone. This formulation should hence give qualitatively different results from before. Another effect to be tested is the effect of the time of virialization of the overdense regions; this was briefly mentioned in the formulation

of mass leak.

Also, we can now check if the mass leak as defined above can lead to an acceleration in the Gaussian model that failed to accelerate. This will, however, require an embedding of multiple regions, and a well-defined notion of nearest neighbours for more than two regions. Ideally, we should embed the spheres in three dimensional space with more than one nearest neighbour. However, the requirement of our spheres being tangential at each time step could induce a vorticity in the displacement of the centres, which would break our global foliation. One way to deal with this would be to consider regions over the homogeneity scale, and embed spheres along a straight line on grounds of statistical isotropy. This would reduce our problem, as a first-approximation, to just each region having two nearest neighbours.

A directed effort must also be made towards formulating a model of mass leak that begins by altering the differential equation itself. It is pertinent to ask when a differential equation with a time-dependent parameter would lead to the same solution as the original differential equation that holds the parameter constant, but updates its initial conditions and parameters at every time step. The two approaches should coincide to a good approximation if the time-variation of the parameter is small enough so as to be held constant in the interval over which we employ the old differential equation. However, this does not tell us what happens when the parameter varies appreciably over any infinitesimal time step.

There is much that can be derived from the notion of proximity that we have defined, in the direction of achieving the coveted light-cone average. The objective would be to quantify the redshift that light experiences as it travels from an emitter to an observer who are separated by some physical distance at the time of emission. Since we haven't an exact profile of densities between two points, we must resort to an ensemble average of all possible density perturbations that the light could pass through in that separation. One way to model this average would be to define a time-dependent probability distribution of the density contrasts and physical radii as the light enters a particular region of space, that is to be employed each time the light successfully traverses that spherical region. This would require the embedding and proximity that we have defined above; the transfer of mass and separation of the two chosen observers being accounted for in the time dependence of our probability distribution function for density, thus replacing a time evolution by an ensemble average. These conditions, and their explicit formulation, would be the ultimate goal of the extension developed in the present thesis. The above heuristic proposition is based on the fact that under the

assumption of spherical collapse as being the model of time-evolution, the state of a density perturbation is defined completely by the density contrast at a particular, specified value of the global EdS time, and the physical radius at that instant of time. This would allow us to calculate a redshift that can then be matched to observations, potentially lending weight to the formalism of inhomogeneity.

Chapter 6

Appendix

A1: The Spherical Collapse Model

The toy models discussed before give us the dynamics of the universe in terms of the dynamics within the individual regions. We must, hence provide a formalism for the evolution of these 'isolated regions'. This is extensively expounded in literature under the jargon of *spherical collapse*; a painfully rigorous treatment can be found in the appendix of [SV04]; a well-motivated and insightful one in [Pad93]. The key formulae are motivated and summarized below, the narrative largely borrowed from [Pad93].

A spherical *top-hat*[1] perturbation is a spherical region in space that has a uniform density that differs from that of the background. The background is typically taken to be an Einstein-deSitter (EdS) universe[2], corresponding to a universe with zero curvature and hence, the critical density. Note that the background can actually be *any* uniform density, not just the critical one. The arguments that follow only make use of a uniform density background until explicitly specified.

Density perturbations in the linear regime are traditionally fourier transformed to obtain corresponding fourier modes of density contrast, the rationale being that the fourier modes of Gaussian random perturbations evolve independently in the linear regime. This convenience is lost in the non-linear regime, and so it is best to deal with the density contrast

[1] the name derives from the shape the plot of density vs radial distance takes – that of an old-timey top hat.

[2] Not to be confused with the Anti-deSitter Universe, the Einstein Universe, the Einstein Static Universe, or the deSitter Universe, all of which are actual paradigms.

in position space itself. Now, the average density in the background will determine the dynamics displayed within the regions of perturbations. This is characterized by the density contrast $\delta := \frac{\rho(x,t)}{\overline{\rho_b(t)}} - 1$, which measures the linear deviation of the perturbation from the average value in the background. An overdense (underdense) region has $\delta > 0\,(< 0)$; $\delta = 0$ corresponds to a spherical region with matching density, and $\delta = -1$ is an empty region.

The background density is assumed to obey the Friedmann dynamics, which is dictated by whether the dimensionless density parameter $\overline{\Omega_b}$ is $<, >$ or $= 1$, corresponding to being lesser than, greater than or equal to the critical density. The critical density evolves as a universe with zero curvature. These follow trajectories of a hyperbola, cycloid, or a $t^{2/3}$ escape velocity profile[3], respectively. Note again, that we are so far describing the possible dynamics of the *background*. A uniform universe with density greater than the critical density will always collapse, as will a universe with lesser than the critical density always remain open. A spherical perturbation withing this region, in the linear regime, will be dragged along with the background behaviour to an extent, but will deviate from the background expansion at a rate that depends on its density contrast. Heuristically speaking, we'd expect a region that is overdense with respect to the background to collapse *with respect to the background*, independent of the value of the background density. This is because it should evolve at a slower rate than the background, thus 'collapsing' relative to its coordinates, despite being initially dragged along with it. Of course, this perturbation need not collapse gravitationally; that would depend on its value relative to the critical density and not the background. These considerations will be made more mathematically precise shortly.

In order to make the formalism analytically tractable, we make use of spherical perturbations in a uniform background. Owing to the spherical symmetry of the region, the dynamics is determined completely by the mass contained with the spherical volume and not the mass outside. The density perturbation at some initial time in coordinates with origin at the centre of the sphere is given by:

$$\rho(r, t_i) = \rho_b(t_i) + \delta\rho(r, t_i) \equiv \rho_b(t_i)(1 + \delta_i(r)), \tag{6.1}$$

where the subscript i on δ denotes the initial time. If the physical size of the perturbation is significantly smaller than the size of the Hubble radius of the background, it turns out

[3]See footnote addressing equation 2.2

that the dynamics of the perturbation are very well approximated by Newtonian equations. To see why this is the case, consider the FRW metric in flat space (the argument holds identically in closed and open spaces as well):

$$ds^2 = -c^2dt^2 + a(t)^2(dx^2 + dy^2 + dz^2).$$

Consider an observer at some point that we shall denote the origin. Then, it is easy to construct a set of *locally inertial* coordinates with respect to that observer, as opposed to the *global* comoving coordinates of the spacelike hypersurface. When the metric is expressed in such a form, it is said to take on the *FRW normal coordinates*. The coordinates are constructed by observing that (i) the observer is freely falling (i.e., the observer is a geodesic), and (ii) the cosmological time t coincides with the observer proper time τ. This can then be used to define a change in basis by considering a light signal emitted by the observer, to be reflected by a mirror at some normal coordinate x and received by the observer again. This is then related to the globally comoving coordinate χ of the mirror. A derivation of this thought experiment can be found here. When this coordinate transformation is expanded in powers of c, we choose to retain terms only upto order c^2 in the denominator. Under such an approximation (which corresponds physically to considering perturbations or distances much smaller than the Hubble radius), the metric takes the form:

$$ds^2 \approx -c^2\left(1 + \frac{2\phi_b(r,t)}{c^2}\right)dt^2 + (dx^2 + dy^2 + dz^2), \tag{6.2}$$

where

$$\phi_b(r,t) = -\frac{1}{2}\frac{\ddot{a}}{a}r^2; \quad r(t) = a(t)\chi.$$

Notice how this change of coordinates alongside the truncated approximation on powers of c allows for a natural weak-field limit approximation. Therefore, to the lowest non-trivial order, we may treat $\phi_b(r,t)$ as an effective Newtonian potential due to the background density. We thus import from the Friedmann equation a relation between the background expansion factor and the value of the background density. This then gives us the effective Newtonian potential in terms of the background density.

Okay! This somewhat lengthy digression aside, we have arrived at a nifty and expedient result: for perturbations of small physical size relative to the Hubble radius, our problem reduces to solving a Newtonian gravitational potential problem for radial motion, that depends only on the value of the density inside the region relative to the critical density. In particular, we may write:

$$\phi_{tot}(r,t) = \phi_b(r,t) + \delta\phi(r,t) = -\frac{1}{2}\frac{\ddot{a}}{a}r^2 + \delta\phi(r,t) = \frac{2\pi}{3}G\rho_b r^2 + \delta\phi(r,t). \tag{6.3}$$

Here, $\delta\phi(r,t)$ is the extra potential generated by the density perturbation $\delta\rho(r,t)$. We may now write down Newton's second law naively, to obtain:

$$\frac{d^2r}{dt^2} = -\nabla\phi_{tot} = -\frac{4\pi G\rho_b}{3}r - \nabla(\delta\phi) = -\frac{GM_b}{r^3}r - \frac{G\delta M(r,t)}{r^3}r = -\frac{GM_{tot}}{r^2}. \tag{6.4}$$

The equalities above hold irrespective of whether our perturbation profile is uniform or not. In going to the last expression, we made use of Gauss' law for inverse-square-law fields to substitute the total mass contained in the perturbation, independent of its arrangement inside. Of course, our considerations are restricted to top-hat perturbation profiles, and so the statement holds more trivially.

It is well known that the trajectory in time for a body travelling at a velocity equal to, greater than, or lesser than the escape velocity is that of a parabola, hyperbola and ellipse, respectively. In the absence of angular velocity (as is the case in the absence of shear and vorticity), the trajectory is purely radial, and the trajectories have a profile of $t^{2/3}$, a hyperboloid and a cycloid, respectively. The conditions for each of the trajectories is more rigorously obtained from the first integral of motion:

$$\frac{1}{2}\left(\frac{dr}{dt}\right)^2 - \frac{GM}{r} = E.$$

This gives us a natural segregation with respect to the sign of E. We need only to explicitly find its functional form in terms of the density contrast to make concrete the statements that were hand-wavily made at the beginning of this section. In order to evaluate E, we recognise that at any instant of time, the mass within the perturbation remains constant, and so the

potential energy can be evaluated at any time. At some initial time t_i, if the perturbation is small, we have the added benefit that the velocity in the kinetic term coincides with the expansion of the background. This allows us to express the kinetic term in terms of the background expansion velocity alone, neglecting to a good enough approximation the radial peculiar velocity due to the additional mass inside. Subscripting all quantities at the initial time by i, we obtain $\dot{r_i} = H_i r_i$, and so

$$K_i = \frac{1}{2} H_i^2 r_i^2.$$

and

$$U_i = -\frac{GM_{tot}}{r_i} = -G\frac{4\pi}{3}\rho_b(t_i) r_i^2 (1+\delta_i) = -\frac{1}{2} H_i^2 r_i^2 \Omega_i (1+\delta_i) = -K_i \Omega_i (1+\delta_i),$$

where Ω_i is the dimensionless density parameter of the background universe relative to the critical value. The total energy is hence given by:

$$E = K_i \Omega_i [\Omega_i^{-1} - (1+\delta_i)]. \tag{6.5}$$

The condition for collapse then becomes $E < 0$, or $\delta_i > (\Omega_i^{-1} - 1)$. Recall that δ is the dimensionless density contrast of the perturbation relative to the average value of the background, while Ω is the dimensionless density parameter of the background relative to the critical EdS universe. For a background that is either critical or closed ($\Omega_i \geq 1$), *any* overdensity δ measured *relative to the background* will collapse. If the background is open ($\Omega_i < 1$), then an overdensity δ measured relative to the background must cross a further threshold ($\delta_{crit} = \Omega_i^{-1} - 1$) to achieve a negative energy, and hence collapse. This threshold value just ensures that the absolute value of the density within the region of consideration is greater than the EdS critical density, as our intuition would suggest.

For the considerations of our toy model, we shall assume an EdS background, corresponding to $\Omega_i = 1$. All the trajectories are parametrized by a *development angle*. The dependence of the radial component on time is obtained by integrating the equations of motion (EOM); the following arguments are made for an overdense region, the formulae for their underdense

counterpart are obtained by switching out all trigonometric functions for corresponding hyperbolic ones. The EOM for $E < 0$ integrate to give:

$$r = A(1 - \cos\theta), \quad t + T = B(\theta - \sin\theta); \quad A^3 = GMB^2, \tag{6.6}$$

where A and B are constants that depend on the initial density contrast. The coordinate r here is the physical radius of our perturbation, not the comoving one. The time offset T is our freedom to choose an initial condition; it can be used to set the initial radius r_i at some $t = t_i$. This is done by inverting the equation of r to obtain θ_i as a function of r_i, and then substituting it in the equation for t with the known t_i to get T. Notice that to have an initial radius at the zero of our time, we must offset our time's origin, because the equations impose the condition that at the global origin of time, all radii go to zero. The reason for this is that at an early enough time, the region of perturbation must coincide with the average density of the background; and since we begin with a universe that is maximally symmetric with perturbations seeded by quantum fluctuations, the perturbations and distances must all go to zero at the global origin of time. The effect of an offset is seen easily below:

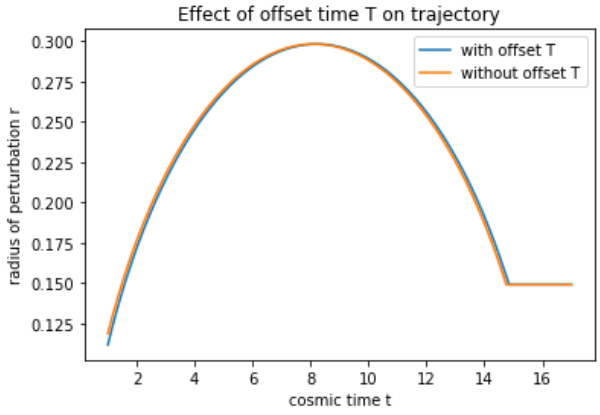

Figure 6.1: Physical radius of region vs cosmic time t plotted for an overdensity of $\delta = 0.6$. The initial conditions were $r_i = 0.11$ at $t_i = 0.001$; the calculated offset was $T = -0.0966$. Note that the trajectory is simply shifted.

The trajectory described above is the parametrized equation of a cycloid[4]. The radius of turnaround is the maximum radius r_m, which is at $\theta = \pi$. The kinetic energy at turnaround

[4]Technically, a cycloid has the same coefficient in the parametrizing equation for both r and t. Think of this as a distorted cycloid.

is zero, and so the total energy is only the potential energy. Taking the ratio of the potential energy at turnaround to the total energy gives us:

$$\frac{r_m}{r_i} = \frac{1+\delta_i}{\delta_i - (\Omega_i^{-1} - 1)}. \tag{6.7}$$

Clearly, $r_m > r_i$, and greater the overdensity, the lesser the radius of turnaround and the faster it is obtained, as our intuition would suggest. Recognising that $r_m = 2A$, we find that:

$$A = \frac{r_i}{2}\frac{1+\delta_i}{\delta_i - (\Omega_i^{-1} - 1)}; \quad B = \frac{1}{2H_i\Omega_i^{1/2}}\frac{1+\delta_i}{[\delta_i - (\Omega_i^{-1} - 1)]^{3/2}}. \tag{6.8}$$

The expression for B is obtained from its relation to A above. For an EdS background, we have $A = \frac{r_i}{2}\frac{1+\delta_i}{\delta_i}$, and $B = \frac{1}{2H_i}\frac{1+\delta_i}{\delta_i^{3/2}}$. The equations finally read:

$$r = \frac{r_i}{2}\frac{1+\delta_i}{\delta_i}(1-\cos\theta), \quad t + T = \frac{1}{2H_i}\frac{1+\delta_i}{\delta_i^{3/2}}(\theta - \sin\theta) \tag{6.9}$$

for an overdense region, and

$$r = \frac{r_i}{2}\frac{1+\delta_i}{(-\delta_i)}(\cosh\theta - 1), \quad t + T = \frac{1}{2H_i}\frac{1+\delta_i}{(-\delta_i)^{3/2}}(\sinh\theta - \theta) \tag{6.10}$$

for an underdense one. Note that for an underdense region relative to an EdS background, $\delta_i < 0$. All other quantities are obtained by taking the relevant derivatives via a repeated application of the chain rule on the development angle.

One final comment on the evolution of overdense regions: since these regions reach a maximum radius and then begin to collapse, their inevitable fate as suggested by the parametrized equation above seems to be to collapse to a singularity in finite time. This, however, is not the observed outcome of the clusters that we see in the night sky. Most overdense structures stabilize to a finite radius post-turnaround. The precise mechanism depends largely on the properties of the matter that our overdensity is composed of: the matter could get thermalized and exert a pressure owing to its newly acquired temperature, or could even radiate energy that contributes to an outward balance to the gravitational collapse. A popular explanation is the phenomenon of *shell-crossing* in the so-called collisionless cold dark matter, which through a process of 'violent relaxation' results in a 'dark matter halo' that

virializes[5] at half the radius of turnaround[6]. This then provides a counter potential that allows the baryonic matter to follow suit and virialize close to the same radius. All these arguments require, crucially, the existence of angular perturbations that induce a vorticity that can further offer an outward centrifugal force. The true stabilizing force can be any combination of the above factors to varying degrees.

Therefore, to preface all the conclusions drawn henceforth in the toy models, the evolution in the individual regions is assumed to be via the spherical collapse model, which (to my best knowledge so far) has no rigorous justification beyond the turnaround of overdense regions. The common consensus is that after turnaround, there is some voodoo dark magic that results in the virialization at half the radius of turnaround. The precise explanation depends on the system being studied, and your choice of religion; numerically, the simulations impose a hard cut-off at $\phi = 3\pi/2$ which results in the graph not being differentiable. A smoother transition can be achieved if there is a smooth asymptotic approach to virialization.

A2: The 2-region model

The following section explores the full scope and implications of the 2-region model that was formulated in [Räs06a] and summarized in Section (3.2.1).

There are three parameters that can be varied in the model: the combination of densities (sign and magnitude), the volume fractions the regions occupy at some particular time, and the time of seeding of these volume fractions.

Also, the following excruciatingly detailed description can be skipped to subsection 3.2.1 where the results are succinctly summarized, and an explanation is attempted.

Varying density

In the following data set, the volume fractions are fixed to a particular value and are seeded at the time of turnaround of the overdense region (when $\phi = \pi$). Three possible volume fractions are considered: $(0.3, 0.7)$, $(0.5, 0.5)$ and $(0.7, 0.3)$, which correspond to allocating a

[5] Dark matter doesn't truly virialize, however, the time scale of its variation is purported to be significantly greater than that of the physics we hope to study that relies on the existence of the halo.

[6] The half radius of turnaround condition is obtained by finding the point at which the kinetic energy is half the potential energy: the condition for virial equilibrium in inverse-square-law forces

greater, equal or lesser volume fraction at turnaround to the underdense region relative to the overdense one. The numerical code calculates the deceleration parameter against cosmic time.

(0.3, 0.7)

These graphs have a volume fraction of 0.7 for the underdense and 0.3 for the overdense region. The first case has the underdense value fixed at -1, that is, it is taken to be empty.

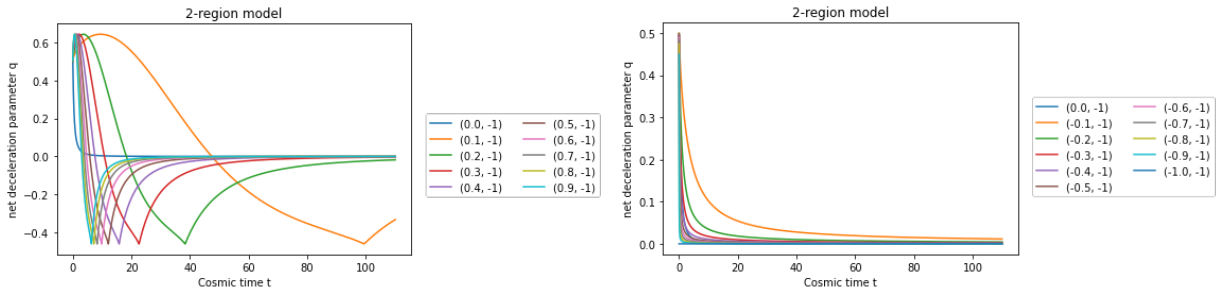

Figure 6.2: Deceleration parameter vs cosmic time t plotted for increasing overdensity and underdensity versus an empty region. The empty region has a volume fraction 0.7 while the underdense and overdense regions have 0.3.

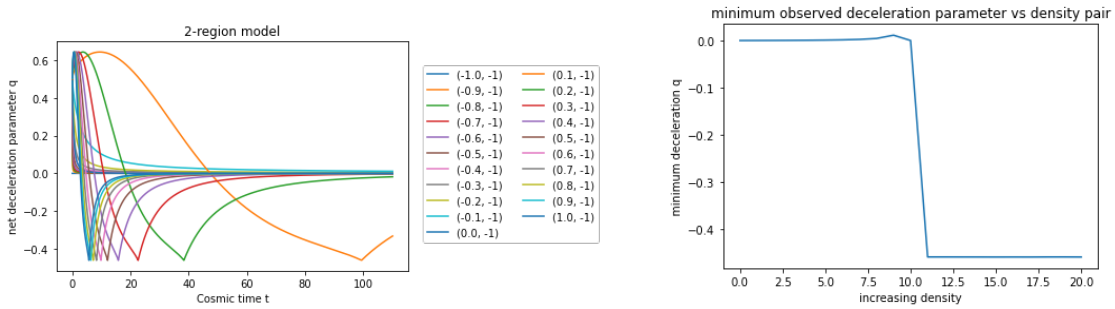

Figure 6.3: Simultaneous plot of over and underdensities, and a graph of the minima obtained vs density pair. In the second graph, as the x-axis increases, we move from under to over densities.

A cursory glance at Figure (6.2) tells us that first, the deceleration parameter takes on negative values only when we pair an overdensity with the empty region; two underdensities do not show an acceleration. Even a critical density value does not show an acceleration. Secondly, the qualitative profile of the deceleration parameter is the same for all overdensities,

in that they first increase to a maximum (deceleration) and then take on negative values. Thirdly, q's maximum and minimum value is largely unaffected by the value of the overdensity. The numerical value of the minima is around -0.459. Underdensities with an empty region are everywhere decelerating and tend to zero asymptotically; the critical density dies out the fastest. This fact, along with a combined plot of overdensity with underdensity for a sense of scale is shown in Fig. (6.3).

As it turns out, the minima is reached at the time of virialization (the abrupt halt in development angle is why the graph is not differentiable), and so the only way the overdensity affects the deceleration parameter is by dictating the time at which the minima is attained. As a result of the non-differentiability of the deceleration parameter, the value of the minima cannot be obtained analytically by differentiation. As expected, a less overdense region takes longer to virialize than a more overdense one, and so q takes longer to attain the same minimum. Note that it is quite possible that the graph has a true minima later; the fact that the overdense regions virialize at $\phi = 3\pi/2$ forces the minima at virialization. We shall return to this point later.

Now consider the underdensity fixed at a value of -0.9 and the other region increasing from critical to overdense.

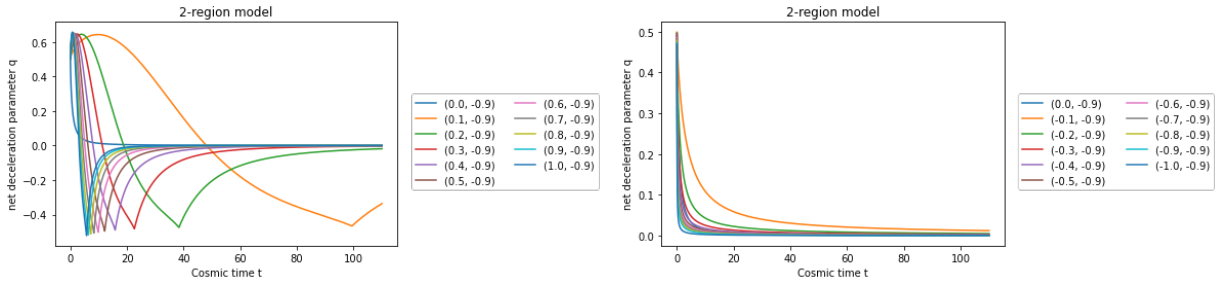

Figure 6.4: Deceleration parameter vs cosmic time t plotted for increasing overdensity and underdensity versus an underdense (-0.9) region.

The first two observations carry over from the previous case of an empty region; here the minimum value of deceleration sees a relatively larger variation with the value of overdensity: a larger acceleration (lower value of q) is seen for a greater overdensity as opposed to a lower overdensity. The variation, however, is still very weak (with a range of 0.06) as compared to

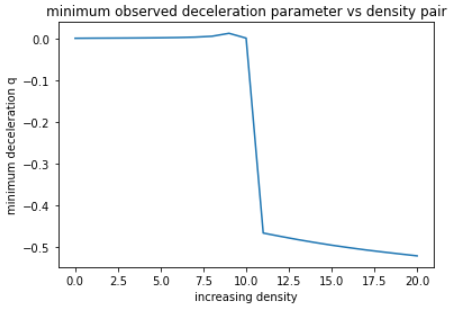

Figure 6.5: Graph of the minima obtained vs density pair. As the x-axis increases, we move from under to over densities.

the effect an underdensity has on the minima of q (as will be demonstrated shortly).

In the next data set, the value of the underdensity is fixed at -0.1 with the same variation effected on the second region. Since the combination of two underdense regions shows the same qualitative behaviour of not accelerating and asymptotically approaching zero, the graph is omitted here.

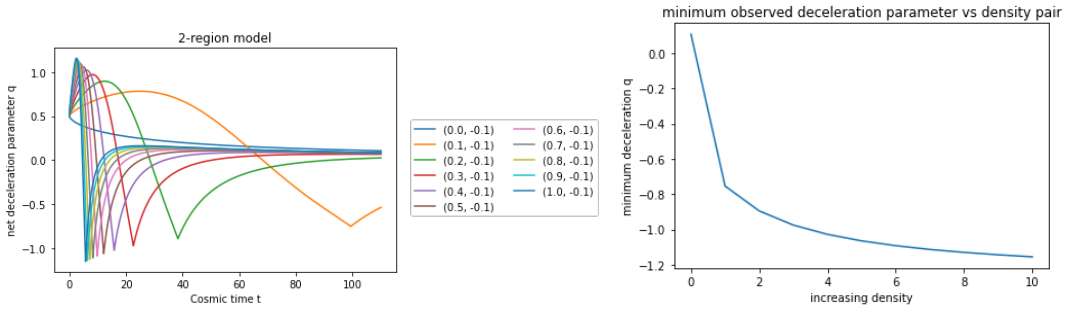

Figure 6.6: The first graph plots the deceleration parameter vs cosmic time t for increasing overdensity versus an underdense (-0.1) region. The second graph is that of the minima obtained vs density pair. As the x-axis increases, we move from less to more overdensities.

All observations carry forward again; the range of minima in this case is 0.4. This is the maximum possible underdensity that can be held constant. The first data point in the graph of minima corresponds to the critical density, which is omitted from the range because it shows no acceleration. Once again, the minima is forced by virialization.

Finally, we study the case of a fixed overdense region with volume fraction 0.3 and a variation in the other region, once again from underdense to overdense.

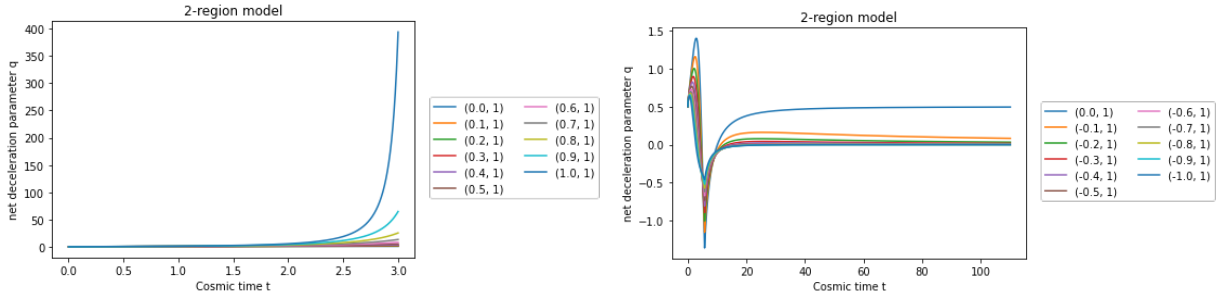

Figure 6.7: Deceleration parameter vs cosmic time t plotted for increasing overdensity and underdensity versus an overdense (1) region.

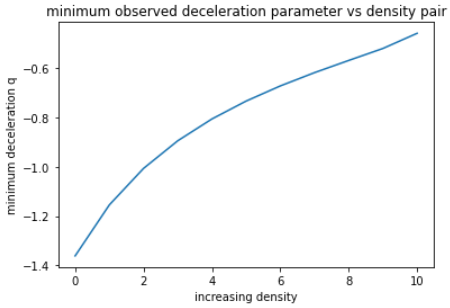

Figure 6.8: Graph of the minima obtained vs density pair. As the x-axis increases, we move from underdense to empty.

Here (Fig.: 6.7, 6.8) we see some variation. Once again, the only combination that leads to an acceleration is when we have an overdense region paired up with an underdense region. Overdensities tend to have divergent positive deceleration parameter values, and so the simulation is carried out for a shorter time value than for the others. The deceleration parameter takes on strictly positive values for two overdense regions. The qualitative profiles are again the same, but now we see that a greater variation in minima is obtained by changing the value of the underdensity by the same increment of 0.1 than for a similar increase in overdensity; the range here is 0.9, which is of order 1. Interestingly, smaller the underdensity, greater the value of the acceleration. q in the cases of higher underdensity becomes positive once more after attaining a minima, but then asymptotically dies out to zero at later times.

(0.5, 0.5)

All the plots above were generated assuming that the underdensity had a dominant volume fraction. The same plots are now generated with an equal volume fraction at the time of seeding, as compiled below.

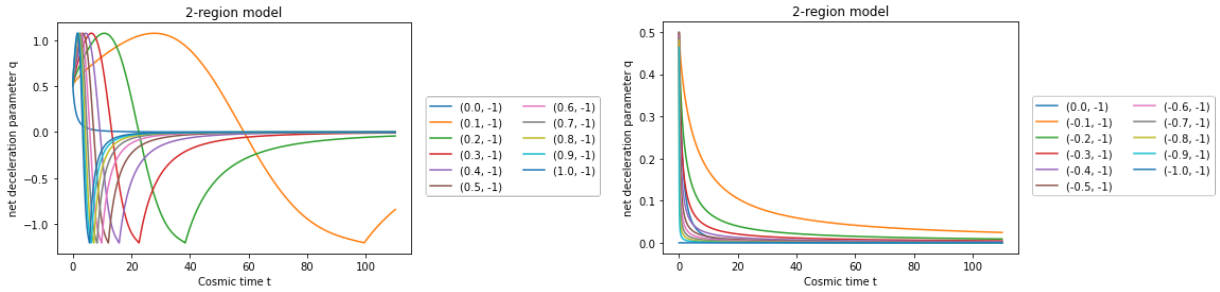

Figure 6.9: Deceleration parameter vs cosmic time t plotted for increasing overdensity and underdensity versus an empty region. The empty and under/overdense regions both have a volume fraction of 0.5.

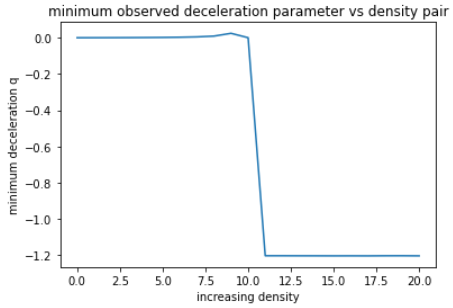

Figure 6.10: Graph of the minima obtained vs density pair. As the x-axis increases, we move from under to over densities.

The conclusions are identical to the empty case before; the minima is per value of overdensity is attained at the same time (since the minima is forced by virialization, which is independent of volume fraction). The minima is constant at -1.2, which is lower than the corresponding minima of -0.459 in the 0.3-0.7 case.

As before, the results do not change qualitatively when the empty region is substituted for a constant underdense one. The effect of the value of overdensities is again more pronounced when the underdensity is lower, but this time, the range is significantly higher.

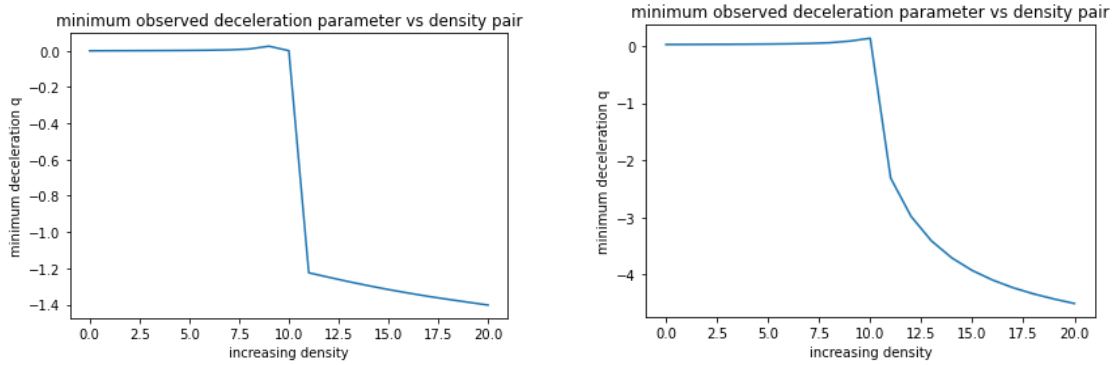

Figure 6.11: Graph of the minima obtained vs density pair. As the x-axis increases, we move from under to over densities. The first graph is for an underdensity of -0.9, while the second for -0.1

Clearly, assigning a greater volume fraction to the overdense region gives it a greater handle over the maximum acceleration obtained. The range of maximum accelerations are 0.2 for an underdensity of -0.9 and 2.2 for an underdensity of -0.1. The acceleration is greater for a more overdense and less underdense region.

Keeping the overdensity fixed at 1, varying the underdensity in the other region gives us Fig.: (6.12).

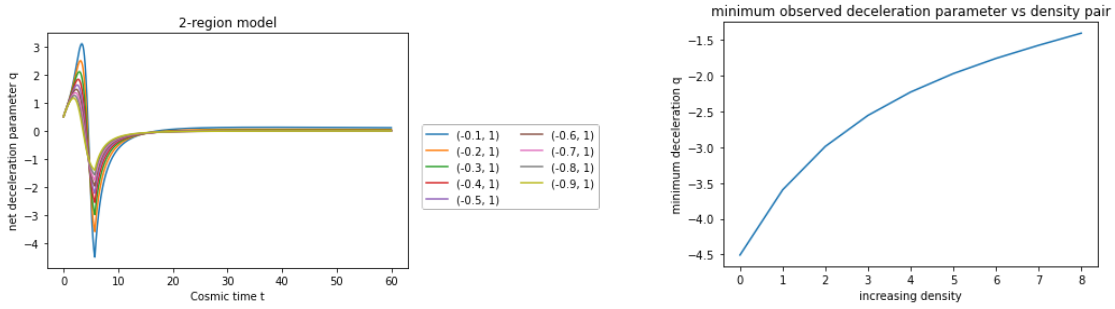

Figure 6.12: q vs t plotted for increasing underdensity versus an overdense region. The second graph is that of the minima obtained vs density pair. As the x-axis increases, we move from less to more underdensities.

The over densities are not plotted against the fixed overdensity because they show no new results (q is everywhere positive). Despite being allocated a lesser volume fraction, the underdense region still has a greater effect on the maximum acceleration than the overdense

regions. The range of $q_{\min}$ here is 4.8.

(0.7, 0.3)

The same analysis is carried out by giving the overdense region a greater volume fraction of 0.7 and the other region a volume fraction of 0.3. The graph is plotted in Fig.: (6.13).

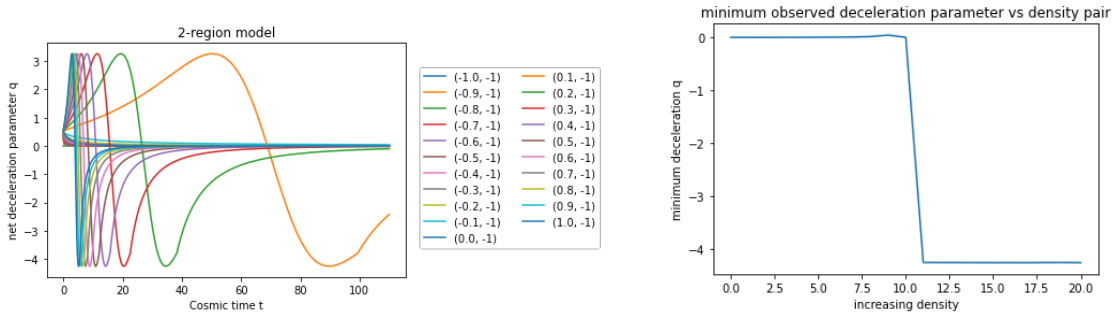

Figure 6.13: q vs t plotted for an empty region and an under/overdense region. The second graph is that of the minima obtained vs density pair. As the x-axis increases, we move from under to overdense regions.

Despite the overdensities being given the dominant volume fraction, we still see an acceleration; the maximum acceleration is a constant at -4.25. Notice here that the minima is attained *before* virialization! So, assigning a greater volume fraction to the overdense regions revokes the command that virialization has over the value of the minima. When plotted against a constant underdensity, the maximum acceleration varies as in Fig.: (6.14).

This is interesting! There is a considerable effect on the value of the overdensity if we give it a greater volume fraction. The range in the second graph of $q_{\min}$ is a staggering 90.3, as opposed to a range of 1 for the first. Note again that the overdensity has a greater effect for a lesser underdensity. When keeping the overdense region fixed at 1, the underdense regions affect the maximum value as in Fig.: (6.15).

Here, the range is 98.6, so while it is still greater than the variation due to overdense regions, the magnitudes are now comparable. Thus, assigning a dominant volume fraction to overdense regions gives them a significant command over the maximum acceleration attainable.

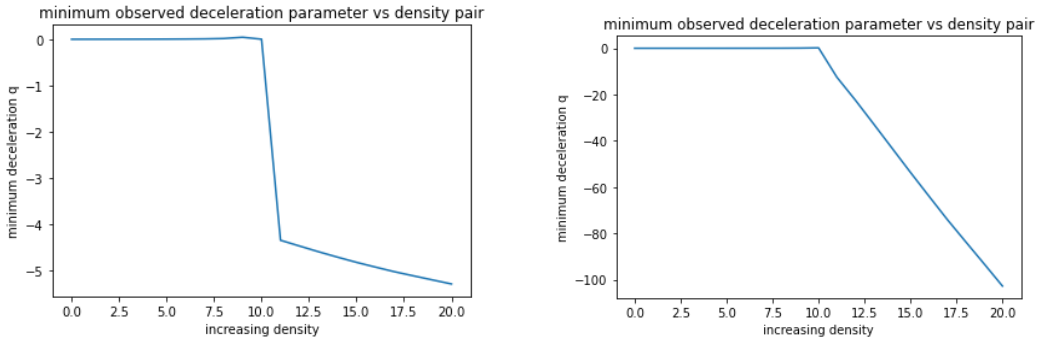

Figure 6.14: Graph of the minima obtained vs density pair. As the x-axis increases, we move from under to over densities. The first graph is for an underdensity of -0.9, while the second for -0.1

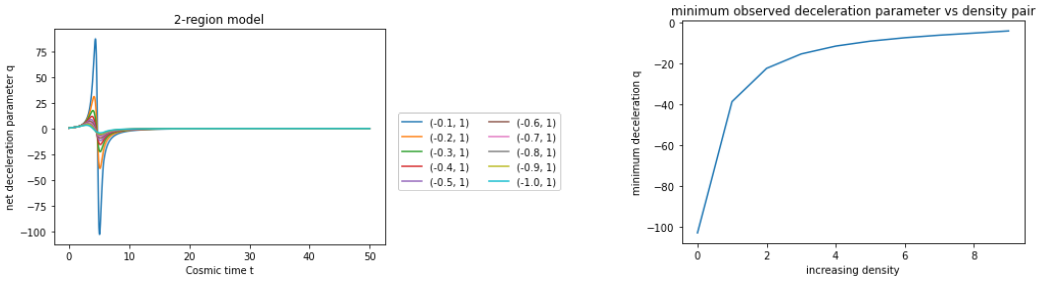

Figure 6.15: q vs t plotted for increasing underdensity versus an overdense region. The second graph is that of the minima obtained vs density pair. As the x-axis increases, we move from less to more underdensities.

Varying volume fractions

In this data set, the volume fraction is varied while keeping the density pairs fixed; the volume fractions are seeded at the time of turnaround of the more overdense region. Five possible density pairs are considered: overdense and empty (1, -1), overdense and underdense (1, -0.9), overdense and less underdense (1, -0.1), overdense and less overdense (1, 0.5) and less underdense and underdense (-0.5, -0.8). The graphs along with the the variation in $q_{\rm min}$ are displayed below from Fig.: (6.16 - 6.20).

In all the plots below, the volume fractions (v_1, v_2) for density contrast values of (δ_1, δ_2) correspond to assigning v_1 to δ_1 and v_2 to δ_2. We see right off the bat that two overdense and two underdense regions can never show an acceleration irrespective of the volume fractions they are imparted. Further, the variation in $q_{\rm min}$ due to changes in volume fraction is significantly greater than any variation seen in the value of densities. In each of the cases, the maximum

acceleration is achieved when a greater volume fraction is imparted to the overdense region. This was also observed in the graphs that varied density values. One interesting trend to note is that as the volume fraction imparted to the overdensities increases, q attains the minima sooner, i.e., before virialization. This was noted in the previous section as well, and is seen more clearly here.

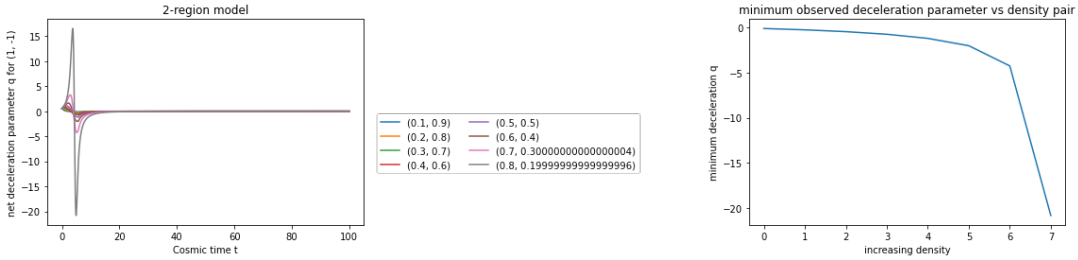

Figure 6.16: q vs t plotted for volume fractions for a density pair of (1, -1). The second graph is that of the minima obtained vs density pair.

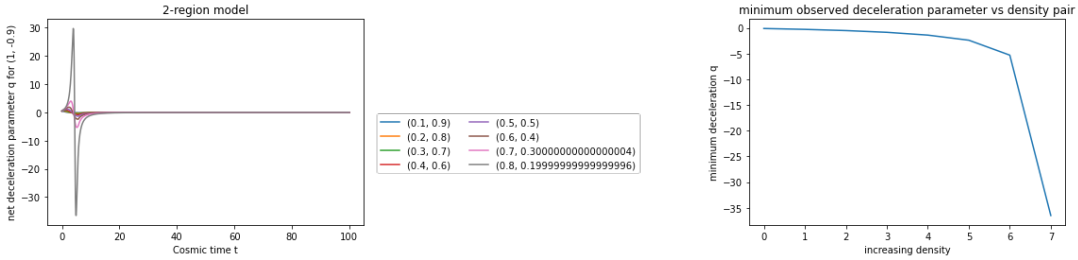

Figure 6.17: q vs t plotted for volume fractions for a density pair of (1, -0.9).

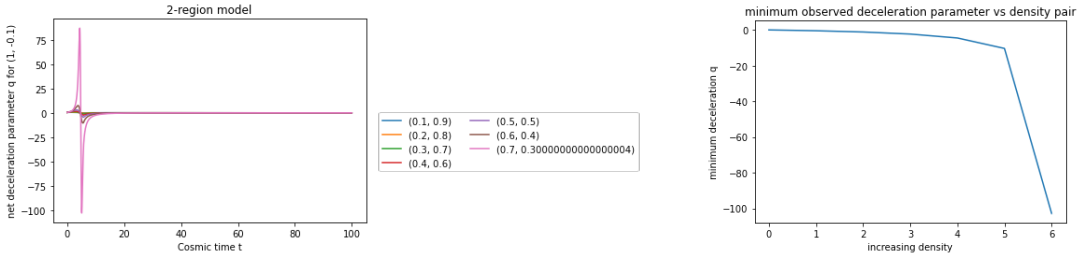

Figure 6.18: q vs t plotted for volume fractions for a density pair of (1, -0.1).

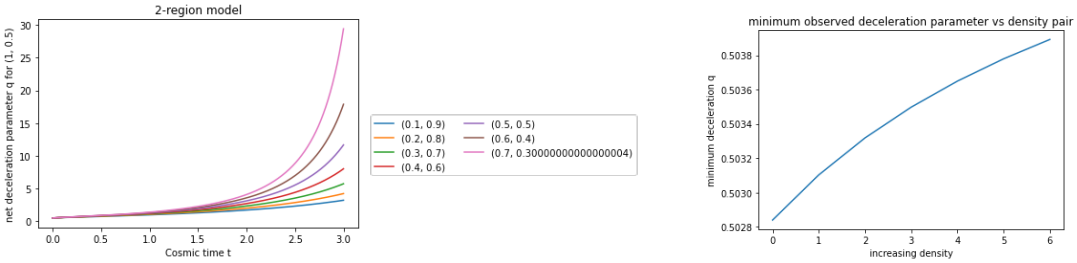

Figure 6.19: q vs t plotted for volume fractions for a density pair of (1, 0.5).

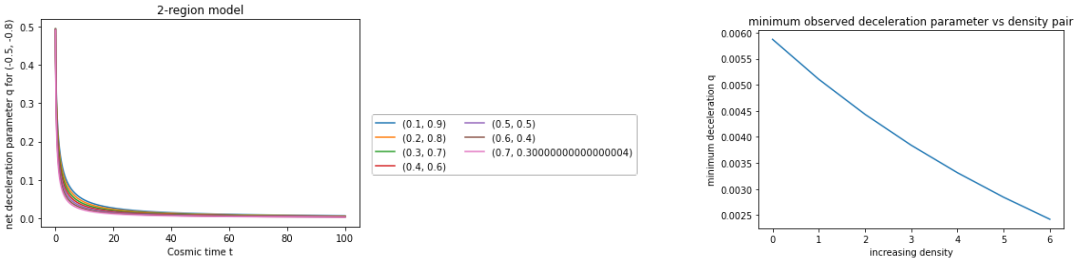

Figure 6.20: q vs t plotted for volume fractions for a density pair of (-0.8, -0.5).

Varying time of seeding

This parameter is explored better in the n region model in section 3; the objective is to study the effect of imposing the volume fractions at the turnaround of the least (vs) most overdense regions. The rationale behind this is that while the most underdense region's point of turnaround defines the time up to which the inversion of development angle from time remains injective, the least underdense region dictates when all the overdense regions as a whole virialize. After the least underdense region has virialized, all the overdense regions stop affecting the system and effectively freeze in time, leaving the simulation at the mercy of the underdense regions only. This effect can only be studied in the presence of more that one overdensity, which can only be imposed when there are more than 2 regions.

Bibliography

[CL90] J. C. Carvalho and J. A. S. Lima. "Newtonian Version of the Variable Mass Theory of Gravity". In: 21 (Nov. 1990), p. 33.

[MFB92] V.F. Mukhanov, H.A. Feldman, and R.H. Brandenberger. "Theory of cosmological perturbations". In: *Physics Reports* 215.5 (1992), pp. 203–333. ISSN: 0370-1573. DOI: https://doi.org/10.1016/0370-1573(92)90044-Z. URL: https://www.sciencedirect.com/science/article/pii/037015739290044Z.

[Nor92] John D. Norton. "A Paradox in Newtonian Gravitation Theory". In: *PSA: Proceedings of the Biennial Meeting of the Philosophy of Science Association* 1992 (1992), pp. 412–420. ISSN: 02708647. URL: http://www.jstor.org/stable/192853 (visited on 10/25/2022).

[Pad93] T. Padmanabhan. *Structure Formation in the Universe*. 1993.

[MM00] W. H. McCrea and E. A. Milne. "Newtonian Universes and the Curvature of Space". In: *General Relativity and Gravitation* 32.9 (Sept. 2000), pp. 1949–1958. DOI: 10.1023/A:1001949117817.

[Mil00] E. A. Milne. "A Newtonian Expanding Universe". In: *General Relativity and Gravitation* 32.9 (Sept. 2000), pp. 1939–1948. DOI: 10.1023/A:1001997000979.

[SV04] Ravi K Sheth and Rien Van De Weygaert. "A hierarchy of voids: much ado about nothing". In: *Monthly Notices of the Royal Astronomical Society* 350.2 (2004), pp. 517–538.

[Räs06a] Syksy Räsänen. "Accelerated expansion from structure formation". In: *Journal of Cosmology and Astroparticle Physics* 2006.11 (2006), p. 003.

[Räs06b] Syksy Räsänen. "Constraints on backreaction in dust universes". In: *Classical and Quantum Gravity* 23.6 (2006), p. 1823.

[BC08] Thomas Buchert and Mauro Carfora. "On the curvature of the present-day Universe". In: *Classical and Quantum Gravity* 25.19 (2008), p. 195001.

[Räs08a] Syksy Räsänen. "Evaluating backreaction with the peak model of structure formation". In: *Journal of Cosmology and Astroparticle Physics* 2008.04 (2008), p. 026.

[Räs08b] Syksy Räsänen. "The effect of structure formation on the expansion of the universe". In: *International Journal of Modern Physics D* 17.13n14 (2008), pp. 2543–2548.

[BR12] Thomas Buchert and Syksy Räsänen. "Backreaction in late-time cosmology". In: *Annual Review of Nuclear and Particle Science* 62 (2012), pp. 57–79.

[EMM12] George F. R. Ellis, Roy Maartens, and Malcolm A. H. MacCallum. *Relativistic Cosmology*. Cambridge University Press, 2012. DOI: 10.1017/CBO9781139014403.

[Mag12] Stefano Magni. "Backreaction and the covariant formalism of general relativity". In: *arXiv preprint arXiv:1202.0430* (2012).